© 2015. Published by The Company of Biologists Ltd | Development (2015) 142, 3746-3757 doi:10.1242/dev.119909

RESEARCH ARTICLE

EMX1 regulates NRP1-mediated wiring of the mouse anterior cingulate cortex

Jonathan W. C. Lim[1,*], Amber-Lee S. Donahoo[1,*], Jens Bunt[1], Timothy J. Edwards[1], Laura R. Fenlon[1], Ying Liu[1], Jing Zhou[5], Randal X. Moldrich[1], Michael Piper[1,3], Ilan Gobius[1], Timothy L. Bailey[4], Naomi R. Wray[1], Nicoletta Kessaris[2], Mu-Ming Poo[5], John L. R. Rubenstein[6,7] and Linda J. Richards[1,3,‡]

ABSTRACT

Transcription factors act during cortical development as master regulatory genes that specify cortical arealization and cellular identities. Although numerous transcription factors have been identified as being crucial for cortical development, little is known about their downstream targets and how they mediate the emergence of specific neuronal connections via selective axon guidance. The EMX transcription factors are essential for early patterning of the cerebral cortex, but whether EMX1 mediates interhemispheric connectivity by controlling corpus callosum formation remains unclear. Here, we demonstrate that in mice on the C57Bl/6 background EMX1 plays an essential role in the midline crossing of an axonal subpopulation of the corpus callosum derived from the anterior cingulate cortex. In the absence of EMX1, cingulate axons display reduced expression of the axon guidance receptor NRP1 and form aberrant axonal bundles within the rostral corpus callosum. EMX1 also functions as a transcriptional activator of *Nrp1* expression *in vitro*, and overexpression of this protein in *Emx1* knockout mice rescues the midline-crossing phenotype. These findings reveal a novel role for the EMX1 transcription factor in establishing cortical connectivity by regulating the interhemispheric wiring of a subpopulation of neurons within the mouse anterior cingulate cortex.

KEY WORDS: Anterograde tracing, Axon guidance, Cerebral cortex, Corpus callosum, *In utero* electroporation, Tractography

INTRODUCTION

The anterior cingulate cortex in humans and mice is particularly important for the performance of executive functions and emotional processing (Gasquoine, 2013; Kim et al., 2014; Meechan et al., 2015). It comprises multiple subdivisions, each with distinct functions that are conferred by differing input and output projections (Vogt and Paxinos, 2014). However, little is known about the development and molecular regulation of the input and output projections of the anterior cingulate cortex.

[1]The University of Queensland, Queensland Brain Institute, Brisbane 4072, Australia. [2]Wolfson Institute for Biomedical Research and Department of Cell and Developmental Biology, University College London, London WC1E 6BT, UK. [3]The University of Queensland, The School of Biomedical Sciences, Brisbane 4072, Australia. [4]The University of Queensland, Institute for Molecular Bioscience, Brisbane 4072, Australia. [5]Institute of Neuroscience, State Key Laboratory of Neuroscience, Shanghai Institutes for Biological Sciences, Chinese Academy of Sciences, Shanghai 200031, China. [6]Nina Ireland Laboratory of Developmental Neurobiology, University of California, San Francisco, San Francisco, CA 94143, USA. [7]Department of Psychiatry, University of California, San Francisco, San Francisco, CA 94143, USA.
*These authors contributed equally to this work

[‡]Author for correspondence (richards@uq.edu.au)

Received 15 November 2014; Accepted 3 September 2015

Homotopic commissural projections from the anterior cingulate cortex are the first axons to cross the midline during corpus callosum development. These cells are primarily born between embryonic day (E) 13 and E14 in mice, and project their axons across the midline at E15.5 (Rash and Richards, 2001; Choe et al., 2012). As the first axons to navigate the complex midline environment during callosal development, these axons are thought to pioneer the initial trajectory that subsequently guides neocortical callosal axons across the midline from E16.5 (Ozaki and Wahlsten, 1998; Rash and Richards, 2001; Richards et al., 2004). Thus, defects in cingulate callosal axon pathfinding are likely to result in malformation of the corpus callosum, which is a relatively common neurodevelopmental disorder in humans (Richards et al., 2004; Paul et al., 2007; Edwards et al., 2014).

Neuropilin 1 (NRP1) and its ligands semaphorin (SEMA) 3A and SEMA3C are involved in the axon guidance of cingulate callosal neurons. NRP1 is expressed on cingulate callosal axons in both humans and mice (Ren et al., 2006; Piper et al., 2009). SEMA3A, which is expressed in a high lateral to low medial gradient in the neocortex during callosal development (Tamamaki et al., 2003; Zhao et al., 2011), is chemorepulsive to cingulate callosal neurons in mice (Piper et al., 2009). By contrast, SEMA3C is expressed by glutamatergic guidepost neurons at the midline, and is attractive to these axons (Niquille et al., 2009; Piper et al., 2009). We have also reported previously that cingulate callosal axons are misguided in mice with a mutated NRP1 receptor that lacks the semaphorin-binding domain ($Nrp1^{Sema-}$ knock-in mice), demonstrating that these molecules are required for the correct guidance of cingulate axons across the midline (Piper et al., 2009).

The empty spiracles homeobox (EMX) transcription factors, EMX1 and EMX2, have been implicated in the development of the anterior cingulate cortex in mice (Pellegrini et al., 1996; Piper et al., 2009). EMX2 regulates the development of the caudal and medial regions of the telencephalon (Pellegrini et al., 1996; Yoshida et al., 1997; Bishop et al., 2000; Mallamaci et al., 2000), whereas much less is known about the function of EMX1 in forebrain development, as *Emx1* knockout brains appear relatively normal (Qiu et al., 1996; Yoshida et al., 1997). However, as *Emx1*; *Emx2* double knockout mice display a more severe phenotype than either single mutant alone, it is likely that the EMX transcription factors function cooperatively in some aspects of cortical development, and that EMX2 may act as a compensatory factor in the absence of EMX1 (Yoshida et al., 1997; Bishop et al., 2002, 2003; Shinozaki et al., 2002; Shinozaki et al., 2004).

Originally, two *Emx1* knockout mouse strains were generated in different laboratories, using either 129/SvJ or (F)1 CBA/C57Bl/6 embryonic stem cells, and both strains exhibit agenesis of the corpus callosum (Qiu et al., 1996; Yoshida et al., 1997). In the most severe cases, callosal axons that normally formed homotopic connections

Development (2015) 142, 3746-3757 doi:10.1242/dev.119909

in the contralateral hemisphere did not cross the midline but projected rostro-caudally within the ipsilateral hemisphere to form aberrant longitudinal bundles called Probst bundles (Probst, 1901; Ren et al., 2007). Subsequently, Guo et al. (2000) generated a third *Emx1* knockout strain using embryonic stem cells derived from the 129/Sv background and backcrossed this strain onto the C57Bl/6 background. They reported that, although the average brain weight of these mice was reduced, the corpus callosum appeared grossly normal, the exception being that its surface area in coronal sections was significantly smaller (Guo et al., 2000). Such phenotypic differences might be due to differences in the targeted insertion constructs used to generate each strain, or more likely the differing genetic backgrounds of these strains (Beck et al., 2000; Sellers, 2012). These conflicting results have led to uncertainty regarding the role of *Emx1* in corpus callosum development.

Here, we report that EMX1 does indeed function to regulate corpus callosum development on the inbred C57Bl/6 background. By crossing the original *Emx1* knockout mice generated by Qiu et al. (1996) onto the C57Bl/6 background, we find that EMX1 is required for the midline crossing of a subpopulation of callosal axons originating from the anterior cingulate cortex, and that these axons form aberrant projections in the absence of EMX1. We demonstrate that EMX1 functions by upregulating the expression of the gene encoding the axon guidance receptor NRP1, thereby establishing a novel regulatory mechanism of NRP1/SEMA signaling in corpus callosum development.

RESULTS

Callosal dysgenesis in *Emx1* knockout mice on the C57Bl/6 background

The role of EMX1 in corpus callosum formation is unclear, as *Emx1* knockout mice generated on different background strains display differing callosal phenotypes (Qiu et al., 1996; Yoshida et al., 1997; Guo et al., 2000). To resolve these differences, we crossed one of the original *Emx1* targeted deletion mutants that displayed agenesis of the corpus callosum (derived with 129/SvJ embryonic stem cells; Qiu et al., 1996) onto a C57Bl/6 background for over ten generations (hereafter referred to as $Emx1^{-/-}$/C57Bl/6). The $Emx1^{-/-}$/C57Bl/6 mice did not display any gross anatomical defects (similar to their pre-backcrossed cousins; Qiu et al., 1996). Congenic analysis of the genomic DNA of the $Emx1^{-/-}$/C57Bl/6 mice demonstrated that they were 95.94% identical to wild-type C57Bl/6 mice.

To analyze whether forebrain commissures cross the midline in adult $Emx1^{-/-}$/C57Bl/6 mice, gold chloride staining was performed on brains bisected at the midline, identical to the analysis performed by Guo et al. (2000). We observed no gross commissural defects of the corpus callosum, hippocampal commissure or anterior commissure in the mid-sagittal plane in any of the genotypes examined (Fig. 1A-C). However, as Probst bundles do not traverse the mid-sagittal plane (Probst, 1901; Ren et al., 2007), we also stained coronal sections for an axonal marker to determine if such bundles were present. Strikingly, neurofilament labeling of axons in serial coronal adult brain sections demonstrated the presence of aberrant axonal bundles in the ventral portion of the corpus callosum (Fig. 1F,I, arrows) that were localized to rostral sections (Fig. 1D-O). Thus, in contrast to the findings of Guo et al. (2000), we observed that adult $Emx1^{-/-}$/C57Bl/6 mice display a subtle but evident callosal dysgenesis phenotype that may provide crucial insight into the function of EMX1 in this system.

EMX1 regulates interhemispheric wiring of the anterior cingulate cortex

As only a subset of callosal axons appeared to be misrouted in $Emx1^{-/-}$/C57Bl/6 mice, we sought to identify whether this subset

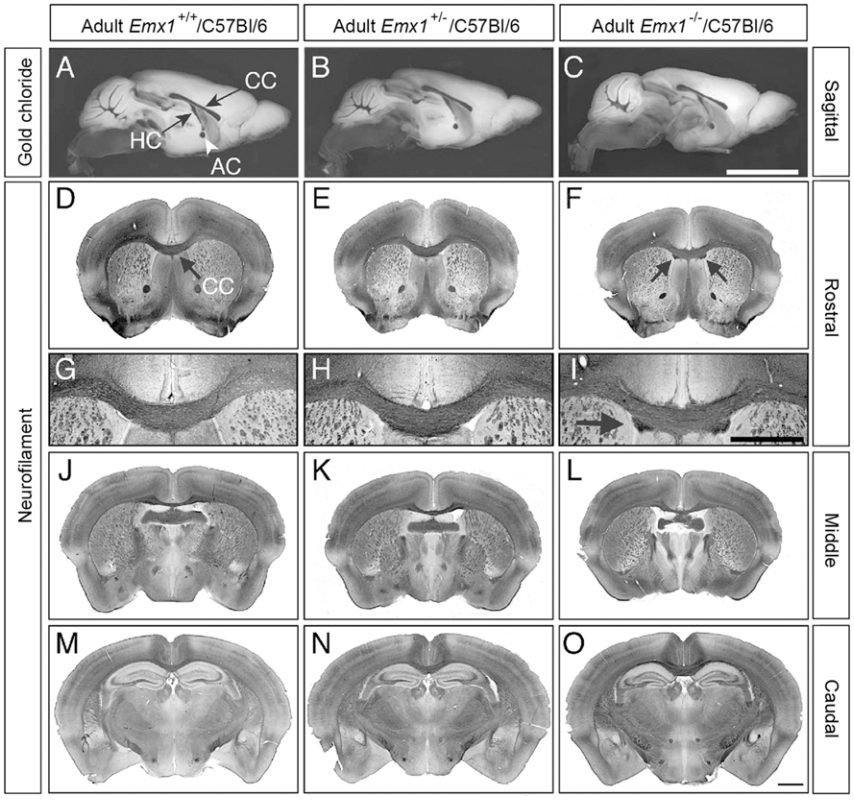

Fig. 1. A subpopulation of callosal axons is disrupted in adult *Emx1* knockout mice. (A-C) Sagittal views of gold chloride staining of adult mouse brains demonstrate the presence of the corpus callosum (CC), anterior commissure (AC) and hippocampal commissure (HC) in all genotypes. (D-O) Neurofilament staining in adult brains, sectioned coronally, revealed the presence of small aberrant bundles in $Emx1^{-/-}$/C57Bl/6 animals, but only in rostral sections (higher power views of D-F are shown in G-I; arrows in F and I indicate the aberrant bundles). *n*=6 per genotype. Scale bars: in C, 5 mm for A-C; in O, 1 mm for D-F,J-O; in I, 1 mm for G-I.

Development (2015) 142, 3746-3757 doi:10.1242/dev.119909

was derived from a single origin, or if it was associated with multiple cortical areas. To investigate this, we used high angular resolution diffusion imaging (HARDI) coupled with tractography to characterize the origin and projection of the aberrant axonal bundles (Moldrich et al., 2010). HARDI is a non-invasive magnetic resonance imaging (MRI) technique that allows the three-dimensional mapping of brain connectivity based on the diffusion of water molecules within axon tracts (Tuch, 2004; Hess et al., 2006). Within each voxel (100 μm^3), the least-restricted direction of water diffusion can be interpreted as the predominant direction of white matter tracts, and represented by different colors on a colored fractional anisotropy (FA) map. Tractography programs then allow regions of interest (ROIs) covering a few voxels to be selected and used as initiation points (or seeds). Streamlines representative of the predominant axonal tract that passes through these ROIs are then reconstructed.

Tractography was initiated from ROIs within the aberrant bundles in adult *Emx1*$^{-/-}$/C57Bl/6 brains, or in equivalent regions of the ventral corpus callosum in *Emx1*$^{+/+}$/C57Bl/6 and *Emx1*$^{+/-}$/C57Bl/6 brains (indicated by the boxed regions in Fig. 2A-C). From sagittal and horizontal views, it is evident that tractography-generated streamlines represent a strong homotopic connection between the anterior cingulate cortices in *Emx1*$^{+/+}$/C57Bl/6 and *Emx1*$^{+/-}$/C57Bl/6 brains (Fig. 2D,E,G,H, green streamlines), whereas streamlines generated from equivalent ROIs in *Emx1*$^{-/-}$/C57Bl/6 brains project rostro-caudally to form aberrant axonal bundles (Fig. 2F,I, purple and blue streamlines). We also generated streamlines passing through an inclusion ROI in the midsagittal corpus callosum, initiated from seed ROIs corresponding to the anterior cingulate cortex, and the primary motor and somatosensory cortices (Fig. 2J-P). This analysis suggests that homotopic connections between the anterior cingulate cortices, but not the primary motor or somatosensory cortices, are reduced in *Emx1*$^{-/-}$/C57Bl/6 animals compared with controls (Fig. 2J-P).

To verify that the aberrant axonal bundles originated from the anterior cingulate cortex, we performed stereotactic iontophoretic injections of an anterograde axonal tracer, biotinylated dextran amine, into adult *Emx1*$^{-/-}$/C57Bl/6 mice and *Emx1*$^{+/+}$/C57Bl/6 controls. In *Emx1*$^{+/+}$/C57Bl/6 controls, callosal axons from the

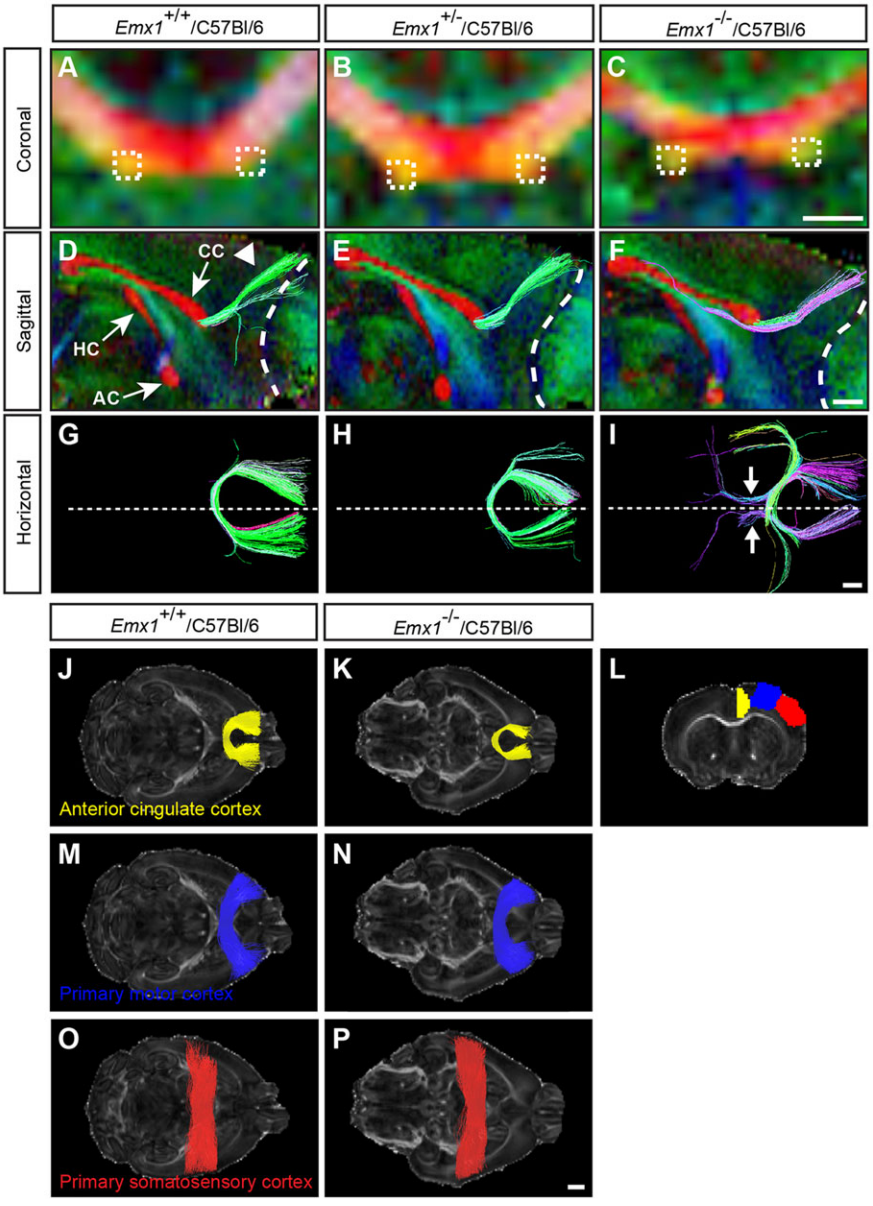

Fig. 2. HARDI and tractography demonstrate that aberrant axonal bundles are associated with the anterior cingulate cortex. (A-C) Colored FA maps were generated in the coronal plane of the rostral corpus callosum using HARDI on adult *Emx1*/C57Bl/6 mice (*n*=5 per genotype). Dashed boxes placed on the aberrant axonal bundles (C) or at anatomically matched regions of the corpus callosum (A,B) represent the ROIs that were traced using Q-ball tractography. (D-F) Sagittal views of the forebrain at the midline (with rostral to the right) represented as colored FA maps with commissural projections shown in red (CC, corpus callosum; HC, hippocampal commissure; AC, anterior commissure), overlaid with tractography streamlines. (G-I) Horizontal view of tractography streamlines, oriented with rostral to the right. Tracts generated from the ROIs in A-C demonstrate streamlines projecting dorso-rostrally (arrowhead in D) into the anterior cingulate cortex in wild type (green streamlines in D,G) and heterozygotes (E,H) whereas in knockout animals the streamlines generated pass through the ROI and run rostro-caudally (purple streamlines in F,I, and arrows in I). Dashed lines in D-F outline the boundary between the olfactory bulb and the cortex, whereas dashed lines in G-I delineate the midline. For all colored FA maps, the predominant direction of white matter tracts is represented by these colors: red, medio-lateral; green, rostro-caudal; blue, dorso-ventral. (J-P) Streamlines were generated in the horizontal plane by seeding ROIs within the anterior cingulate (yellow streamlines), primary motor (blue streamlines), or primary somatosensory (red streamlines) cortex of one hemisphere, and restricting streamlines to those passing through the corpus callosum (*n*=5 per genotype). The coronal section in L demonstrates the seed ROIs from which streamlines were generated. *Emx1*$^{-/-}$/C57Bl/6 mice demonstrate reduced homotopic connections that are specific to the anterior cingulate cortex and not the primary motor or somatosensory cortices. Scale bars: in C, 500 μm for A-C; in F, 2 μm for D-F; in I, 1 μm for G-I; in P, 1 mm for J-P.

Development (2015) 142, 3746-3757 doi:10.1242/dev.119909

anterior cingulate cortex projected through dorsal regions of the corpus callosum to form homotopic connections in the contralateral hemisphere (Fig. 3B-D). Although similar projections were present in the *Emx1*$^{-/-}$/C57Bl/6 mice (Fig. 3A), the labeled cingulate projections were de-fasciculated at the midline, with more cingulate axons projecting through the ventral region of the corpus callosum (Fig. 3E-G) compared with wild-type controls. A subpopulation of labeled axons also contributed to the aberrant axonal bundle, but only within the region ipsilateral to the injection site (Fig. 3F,G, arrowheads). Collectively, these data indicate that ipsilateral projections from the anterior cingulate cortex contribute to the aberrant axonal bundles in *Emx1*$^{-/-}$/C57Bl/6 mice.

Aberrant axonal bundles in *Emx1*$^{-/-}$/C57Bl/6 mice arise during embryonic callosal development

To understand more fully the mechanism underlying the formation of the aberrant axonal bundles in *Emx1*$^{-/-}$/C57Bl/6 mice, we first sought to determine when and how they arise. To investigate this, we performed immunohistochemical analysis for the axonal marker GAP43 on mice at either E17 or postnatal day (P) 0, when the majority of callosal axons would have just crossed the midline. Sections of developing brain from the pre-backcrossed *Emx1*$^{-/-}$/129/SvJ strain demonstrated agenesis of the corpus callosum and the presence of Probst bundles (Fig. 4A,B). In the post-backcrossed *Emx1*$^{-/-}$/C57Bl/6 strain, the aberrant axonal bundles were present in the ventral portion of the corpus callosum in rostral sections, similar to the findings in adult *Emx1*$^{-/-}$/C57Bl/6 brains (Fig. 4C-E). These results demonstrate that, during cortical development, EMX1 is required for the interhemispheric connectivity of a specific subpopulation of callosal axons.

Emx1$^{-/-}$/C57Bl/6 mice lack NRP1 expression in the anterior cingulate cortex

De-fasciculation of cingulate callosal axons has also been reported in mice with specific deletion of *Nrp1* in the primary motor cortex (Zhou et al., 2013), very similar to our observations in *Emx1*$^{-/-}$/C57Bl/6 mice. We therefore hypothesized that NRP1/SEMA signaling might be disrupted in the *Emx1*$^{-/-}$/C57Bl/6 mice. To investigate this, we first sought to determine how these proteins are expressed *in vivo*. We previously showed that NRP1 is expressed in cingulate callosal axons during initial callosal formation (E15-E17; Piper et al., 2009). EMX1 is expressed within the anterior cingulate cortex during a similar period (E14-E16; Fig. 5A-C). In a reporter mouse line expressing tdTomato in *Emx1*-positive cells (*Emx1*-iCre; ROSA26CAG-lox-STOP-lox-tdTomato; Kessaris et al., 2006; Madisen et al., 2010), *Nrp1* mRNA was observed in tdTomato-positive cells in the anterior cingulate cortex at E15, suggesting that EMX1 and NRP1 are co-expressed within cingulate neurons (Fig. 5D-F). To determine if *Nrp1* mRNA expression is altered in the anterior cingulate cortex of *Emx1*$^{-/-}$/C57Bl/6 mice, we dissected E16 brain tissue from the cingulate cortex for real-time quantitative PCR (qPCR) analyses. In the *Emx1*$^{-/-}$/C57Bl/6 mice, *Nrp1* expression was significantly

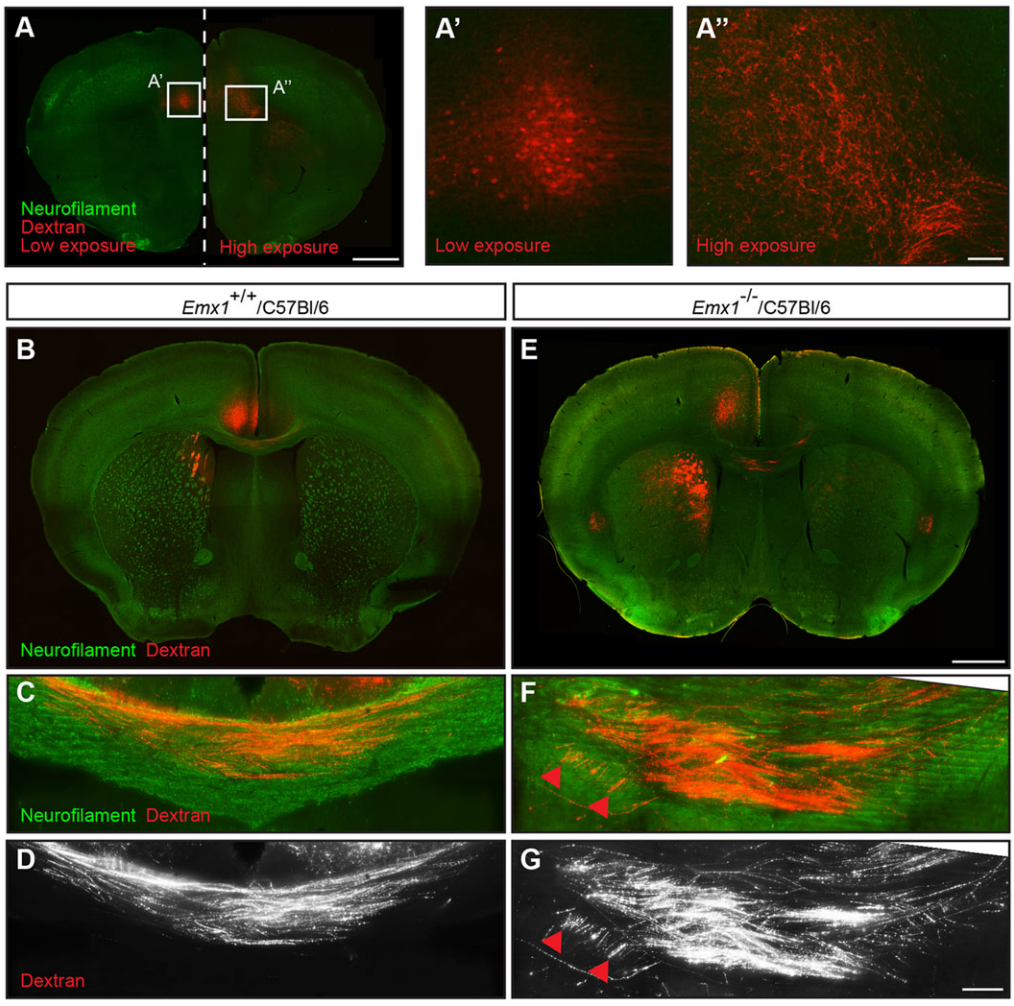

Fig. 3. Anterograde tracing demonstrates that the aberrant axonal bundles in adult *Emx1* knockout mice originate from the anterior cingulate cortex. (A) Iontophoretic injection of biotinylated dextran amine into the anterior cingulate cortex of adult *Emx1*$^{-/-}$/C57Bl/6 mice demonstrates labeled cell bodies at the site of injection (A′) and homotopic projections in the contralateral hemisphere (A″). A′ and A″ represent high-magnification views of the boxed regions in A. (B-G) Cingulate callosal projections at the midline in *Emx1*$^{+/+}$/C57Bl/6 wild-type controls projected through relatively dorsal regions of the corpus callosum (B-D) whereas these axons in *Emx1*$^{-/-}$/C57Bl/6 mice projected through relatively ventral regions of the corpus callosum and contributed to the aberrant axonal bundle within the ipsilateral hemisphere (E-G). *n*=3 per genotype. Red arrowheads indicate labeled axons within the aberrant axonal bundle. Scale bars: in A, 1 mm for A; in A″, 100 µm for A′,A″; in E, 1 mm for B,E; in G, 100 µm for C,D,F,G.

Development (2015) 142, 3746-3757 doi:10.1242/dev.119909

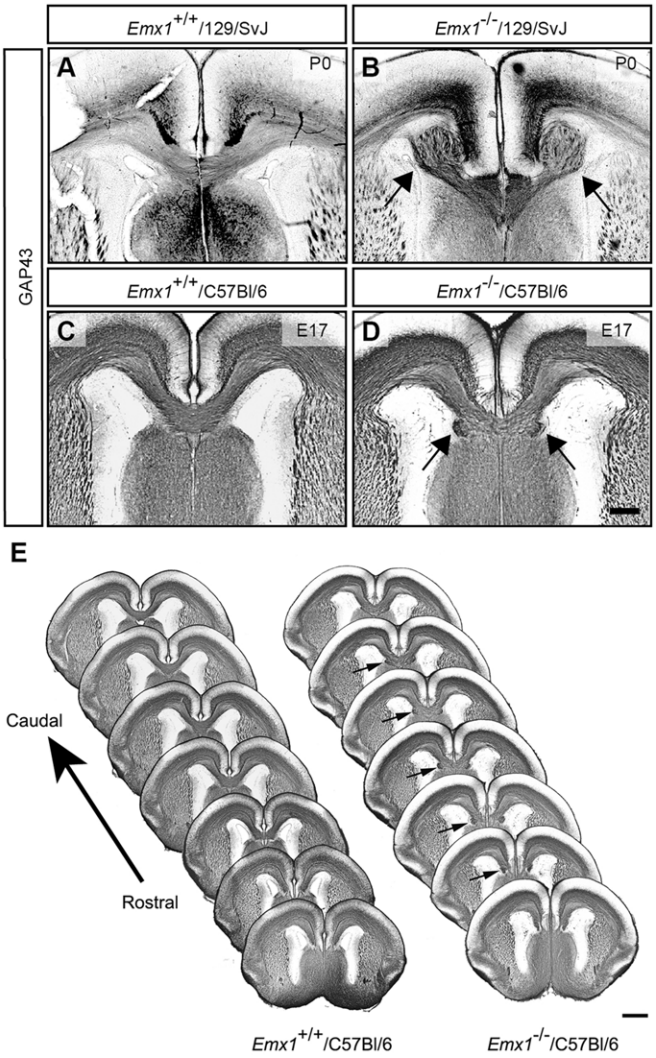

Fig. 4. Aberrant axonal bundles arise during embryogenesis in *Emx1* knockout mice. (A-D) GAP43 staining of *Emx1* knockout brains on the 129/SvJ (A,B) or C57Bl/6 (C,D) backgrounds demonstrates complete agenesis of the corpus callosum and the formation of Probst bundles on the 129/SvJ background (arrows in B), whereas on a C57Bl/6 background, aberrant bundles are present in the ventral portion of the corpus callosum (arrows in D), with most of the structure developing normally (n=4-6 per genotype). (E) A consecutive set of rostral to caudal GAP43-stained sections from one brain at E17 demonstrates that the aberrant bundles are present during embryogenesis in rostral sections of the brain (arrows), where callosal axons are first crossing the midline. Scale bars: in D, 200 µm for A-D; in E, 500 µm.

reduced in $Emx1^{-/-}$/C57Bl/6 mice to ~40% of the levels observed in their wild-type littermates (Fig. 5G).

We next used immunohistochemistry to verify that NRP1 protein expression was similarly reduced, staining E16 coronal brain sections of $Emx1^{-/-}$/C57Bl/6 and $Emx1^{+/+}$/C57Bl/6 littermates. In the $Emx1^{-/-}$/C57Bl/6 mice, the expression of NRP1 was reduced in the cingulate cortex and at the midline where cingulate callosal axons were projecting into the contralateral hemisphere (Fig. 5H-M). This did not appear to be due to an overall decrease of NRP1 expression throughout the brain as NRP1 expression was retained caudally within the hippocampal commissure (Fig. 5M). Thus, $Emx1^{-/-}$/C57Bl/6 mice display reduced NRP1 expression in cingulate callosal axons that are forming the corpus callosum.

Emx1$^{-/-}$/C57Bl/6 cingulate axons are unresponsive to SEMA3C-mediated guidance *in vitro*

To determine whether reduced NRP1 expression in $Emx1^{-/-}$/C57Bl/6 cingulate callosal axons disrupts NRP1/SEMA3C signaling, we performed co-culture assays examining both neurite outgrowth and guidance in explants of cingulate cortex from E15.5 $Emx1^{-/-}$/C57Bl/6 versus $Emx1^{+/+}$/C57Bl/6 mice challenged with HEK293T SEMA3C-overexpressing or control cell blocks. Axons from $Emx1^{+/+}$/C57Bl/6 cingulate cortex were significantly attracted to SEMA3C, as previously shown (Fig. 6A,B,E; Niquille et al., 2009; Piper et al., 2009), whereas this attraction was abolished in explants from $Emx1^{-/-}$/C57Bl/6 mice (Fig. 6C-E). No significant difference in outgrowth was observed between the two genotypes (Fig. 6F). These data demonstrate that the NRP1/SEMA3C-mediated guidance of cingulate axons is disrupted in $Emx1^{-/-}$/C57Bl/6 mice.

EMX1 regulates the expression of *Nrp1 in vitro*

The reduced expression of *Nrp1* mRNA and protein in $Emx1^{-/-}$/C57Bl/6 mice suggests that EMX1 acts as a transcriptional activator of *Nrp1* expression. To test this, we identified potential EMX1 binding sites within the *Nrp1* locus using the web-based tool FIMO (Grant et al., 2011) and consensus EMX1 binding sites represented as position weight matrices (Fig. S1A; Jolma et al., 2013). As EMX1 and NRP1 appear to be similarly required for callosal development in humans (Ren et al., 2006), we examined the *Nrp1* promoter and 5′ untranslated regions (5′ UTR) shared between mouse and human, and identified four highly conserved sequences containing putative monomeric and dimeric EMX1 binding sites (Fig. 7A; Fig. S1B). To determine whether EMX1 is able to regulate *Nrp1* transcription via this region, we cloned the mouse and human *Nrp1* promoters encompassing these sequences to drive a firefly luciferase construct for dual-luciferase reporter assays in U251 MG cells. Overexpression of EMX1 resulted in a fivefold or 6.5-fold increase in *Nrp1* promoter activity from the mouse or human *Nrp1* promoter construct, respectively, compared with overexpression of a GFP control plasmid (Fig. 7B; Fig. S1C). This suggests that EMX1 overexpression is able to upregulate *Nrp1* promoter activity *in vitro*.

In the full-length mouse *Nrp1* promoter construct, three of the identified EMX1 binding sites were located within the 5′ UTR, with the remaining binding site located within the promoter region. To further investigate the role of individual EMX1 binding sites in inducing *Nrp1* promoter activity, we designed truncated firefly luciferase constructs encompassing different regions of the full-length construct. When EMX1 was co-expressed in U251 MG cells *in vitro*, the luciferase construct containing the sole EMX1 binding site within the promoter (denoted 'prom' in Fig. 7B) upregulated *Nrp1* promoter activity to levels resembling those of the full-length *Nrp1* promoter, but this upregulation was abolished when the EMX1 binding site was removed ('prom Δ*s1*' in Fig. 7B). *Nrp1* promoter activity was also significantly upregulated in the truncated promoter and 5′ UTR construct containing all four EMX1 binding sites (denoted '5′ UTR+*s1*'), as well as the truncated 5′UTR containing three EMX1 binding sites (denoted '5′ UTR'). Together, these results suggest that, although the EMX1 binding sites may play an additive role in regulating *Nrp1* promoter activity, the binding site within the *Nrp1* promoter ('*s1*' in Fig. 7B) is most important for upregulating *Nrp1* promoter activity *in vitro*.

NRP1 regulates axonal crossing of cingulate axons *in vivo*

Our findings suggest that EMX1 regulates the expression of *Nrp1* that is required for midline crossing of cingulate axons. To confirm

Development (2015) 142, 3746-3757 doi:10.1242/dev.119909

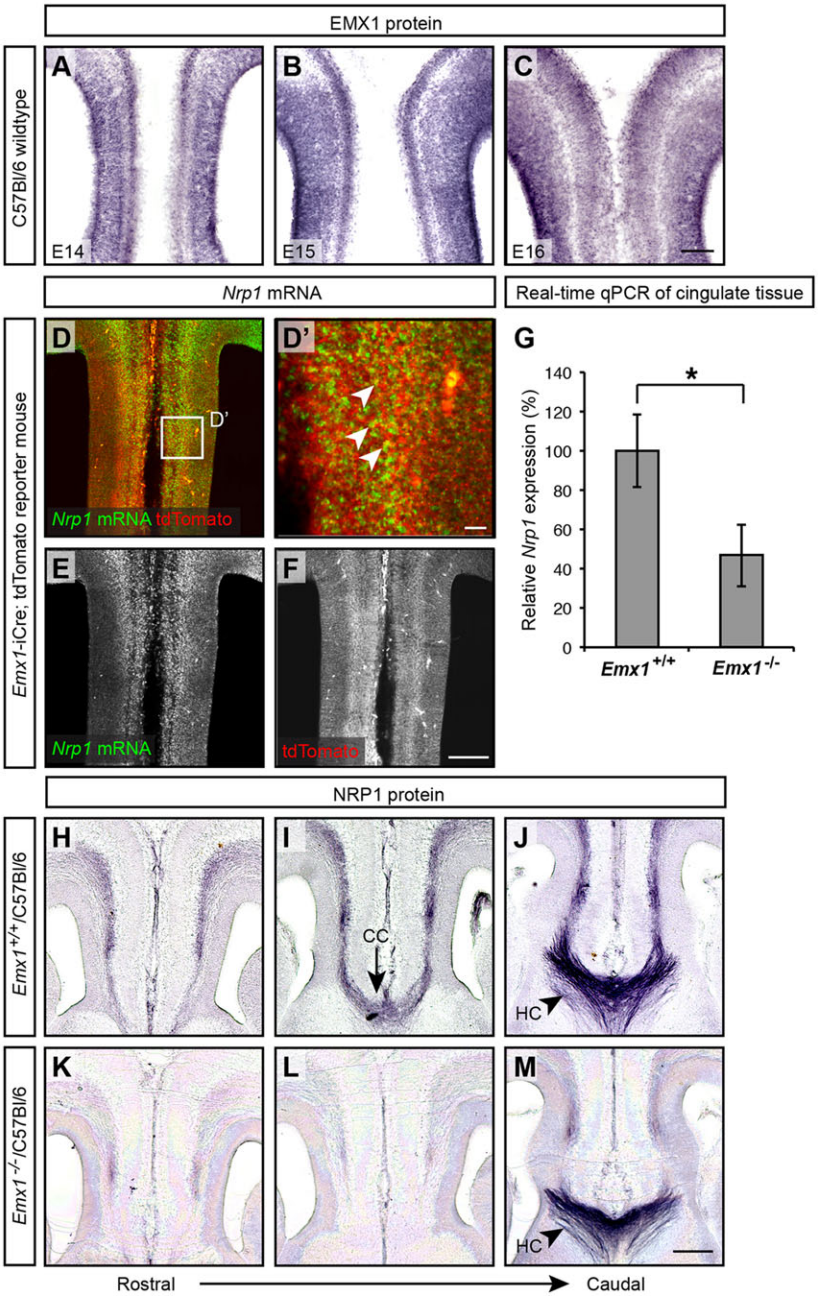

Fig. 5. Expression of EMX1 in the anterior cingulate cortex and reduced NRP1 expression in cingulate callosal axons. (A-C) Coronal sections of C57Bl/6 wild-type brains demonstrate EMX1 protein expression in the anterior cingulate cortex from E14-E16 (n=3 per age group). (D-F) *Nrp1 in situ* hybridization in coronal brain sections of an E15 *Emx1*-iCre; tdTomato reporter mouse (n=3) expressing tdTomato in EMX1-positive cells demonstrates *Nrp1* colocalization with tdTomato within the anterior cingulate cortex (arrowheads in D′). A high-magnification view of the boxed region in D is shown in D′. (G) *Nrp1* mRNA expression in the cingulate cortex of E16 $Emx1^{-/-}$/C57Bl/6 mice was significantly reduced compared with that in $Emx1^{+/+}$/C57Bl/6 controls. *P<0.05; one-sided Wilcoxon rank sum test. *Nrp1* mRNA expression was determined using real-time qPCR, normalized to *Actb* as a housekeeping gene. Results are mean±s.e.m. from n=4 per genotype. (H-M) NRP1 staining demonstrates that NRP1 protein at the cortical midline is similarly reduced in E16 $Emx1^{-/-}$/C57Bl/6 animals (n=3 per genotype). NRP1 is still expressed in the hippocampal commissure (J,M) as seen in caudal sections. CC, corpus callosum; HC, hippocampal commissure. Scale bar: in C, 100 µm for A-C; in D′, 20 µm; in F, 200 µm for D-F; in M, 200 µm for H-M.

this *in vivo*, we specifically removed NRP1 in the cingulate cortex by electroporating $Nrp1^{flox/flox}$ mice with a *Cre*-expressing plasmid at E14.5 (just prior to when cingulate callosal axons begin to project across the midline; Rash and Richards, 2001). Cingulate callosal axons electroporated with either EGFP or *Cre*-EGFP had projected across the midline and into the contralateral hemisphere by P5 in $Nrp1^{WT/WT}$ mice (Fig. 8A,C). This was also evident in the cingulate axons of $Nrp1^{flox/flox}$ mice electroporated with EGFP (Fig. 8B). However, the number of callosal axons crossing the midline and projecting into the contralateral hemisphere was reduced in $Nrp1^{flox/flox}$ mice electroporated with *Cre*-EGFP (Fig. 8D,E). A proportion of these axons instead projected laterally out of the cingulate cortex and away from the midline (Fig. 8D, arrow). These data demonstrate that NRP1 is required for the appropriate guidance of cingulate axons across the corpus callosum *in vivo*, and that a similar reduction of NRP1 expression in the cingulate axons of $Emx1^{-/-}$/C57Bl/6 mice is likely to contribute to the misguidance of cingulate axons observed in these mice.

Expression of *Nrp1* in the cingulate cortex of $Emx1^{-/-}$/C57Bl/6 mice can partially rescue the phenotype

To test directly whether the loss of NRP1 expression downstream of EMX1 was responsible for the pathfinding defects observed in the $Emx1^{-/-}$/C57Bl/6 mice, we performed a rescue experiment by over-expressing *Nrp1* in the cingulate callosal neurons of these mice. To achieve this, cingulate neurons in $Emx1^{-/-}$/C57Bl/6 mice were electroporated at E14 with either *Nrp1* or YFP control plasmid, and the number of sections displaying crossing cingulate axons were blindly quantified at E17 (Fig. 8G,I). In control YFP electroporations of $Emx1^{-/-}$/C57Bl/6 mice, we observed that

Development (2015) 142, 3746-3757 doi:10.1242/dev.119909

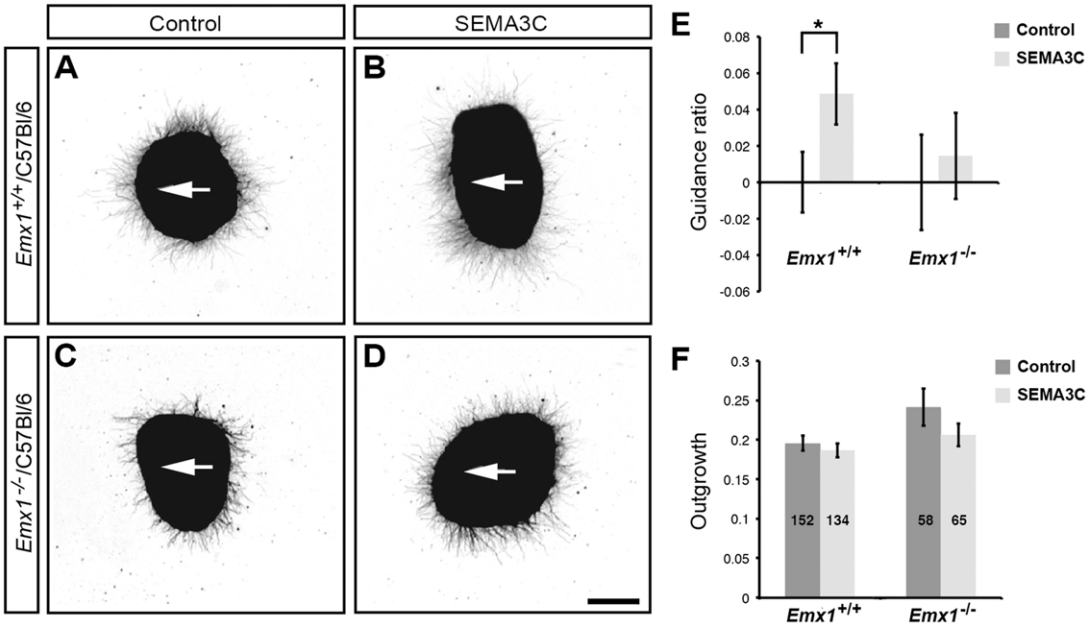

Fig. 6. EMX1 regulates SEMA3C-mediated chemoattraction of callosal axons from the cingulate cortex. (A-D) Cingulate cortical explants were dissected from E15.5 *Emx1*$^{+/+}$/C57Bl/6 and *Emx1*$^{-/-}$/C57Bl/6 mice to examine callosal axon guidance *in vitro*. Explants were co-cultured with either control HEK293T-cell blocks or SEMA3C-expressing HEK293T-cell blocks (white arrows point towards the cell blocks). (E) Explants from *Emx1*$^{+/+}$/C57Bl/6 animals were significantly attracted by SEMA3C-expressing cell blocks compared with control cell blocks. By contrast, SEMA3C did not significantly attract axons from *Emx1*$^{-/-}$/C57Bl/6 cingulate cortex. (F) Outgrowth of cingulate cortical axons was unaffected by SEMA3C. All SEMA3C guidance values were normalized to control values in E. Total explant *n* values pooled from three independent experiments are displayed within the columns in F. *P<0.05 for two-tailed Student's *t*-test. Results are mean±s.e.m. Scale bar: in D, 200 µm for A-D.

76% (62/82) of sections contained YFP-positive cingulate axons that crossed the midline by E17, substantiating our anterograde tracing experiments that demonstrated significant midline crossing in these mice. Despite this, in *Emx1*$^{-/-}$/C57Bl/6 mice electroporated with *Nrp1*, we observed a significant increase in the number of sections in which *Nrp1*-electroporated axons crossed the midline (88%; 72/82 sections) compared with that in control YFP-electroporated brains (P<0.05, one-sided Fisher's exact test, n=18 per condition). These data provide evidence that restoring *Nrp1* expression to cingulate neurons at E14 is sufficient to partially rescue the cingulate axon guidance phenotype of *Emx1*$^{-/-}$/C57Bl/6 mice. We also found that *Emx1*$^{+/+}$/C57Bl/6 cingulate neurons electroporated with *Nrp1* at E14 showed no differences in pathfinding by E17 when compared with YFP electroporations (Fig. 8F,H), suggesting that ectopic over-expression of *Nrp1* does not disrupt midline guidance of cingulate callosal neurons.

DISCUSSION

The anterior cingulate cortex is part of a forebrain network that is required for processing emotion-related behaviors, including aggression, depression, self-esteem, pain and stress (Vogt, 2005; Weber et al., 2006; Toth et al., 2012; Yamashita et al., 2013; Agroskin et al., 2014). The molecular regulation of its development, and particularly its role in corpus callosum development, are only now becoming evident (Niquille et al., 2009; Piper et al., 2009). Here, we have provided evidence that *Emx1* knockout mice display a subtle callosal dysgenesis phenotype that is associated with this brain region. Our findings demonstrate a novel role for EMX1 in regulating the pathfinding and fasciculation of callosal axons originating from the anterior cingulate cortex.

The callosal phenotype of *Emx1* knockout mice is affected by background strain

Our findings in the present study are in contrast to those of Guo et al. (2000), who analyzed a similar *Emx1* null mutant on the C57Bl/6 background. These differences may be explained by discrepancies in the method of analysis. Specifically, Guo and colleagues used Nissl-stained coronal sections and gold chloride staining of mid-sagittally bisected brains for their analysis. Similar to their findings, we also observed no phenotype when we analyzed our *Emx1*$^{-/-}$/C57Bl/6 brains with gold chloride staining. However, upon further analysis with an axonal marker, we were able to demonstrate aberrant axonal bundles that originated from the anterior cingulate cortex. Similar analyses of the strain studied by Guo et al. (2000) would determine if it shares an identical phenotype.

Taken together with the previous studies that analyzed *Emx1* null mutants on mixed backgrounds (Qiu et al., 1996; Yoshida et al., 1997), our findings demonstrate that the severity of callosal dysgenesis in these mice is dependent on genetic background. In humans, different callosal malformations have been observed in patients with similar genetic etiologies, suggesting that modifier genes are likely to influence the severity of this condition (Schaefer et al., 1997; Dastot-Le Moal et al., 2007; Edwards et al., 2014). The effects of genetic background have also been previously described for a number of other genes in the mouse central nervous system, including *Scn1a* (Miller et al., 2014) and *Gnaz* (van den Buuse et al., 2007). In these cases, quantitative trait locus mapping, coupled to gene expression and phenotypic analyses have identified the modifier loci and encompassing genes that might mediate these effects. Similar experiments using the *Emx1*$^{-/-}$/C57Bl/6 and *Emx1*$^{-/-}$/129/SvJ mouse models could identify the modifier loci influencing EMX1-mediated callosal dysgenesis. In turn, genes within the modifier loci themselves may

Development (2015) 142, 3746-3757 doi:10.1242/dev.119909

A

	Binding sequence	Site location	p-value
Mouse *s1*	GGCAATCACT	-127 to -118	0.00778
Human	GGCAATTACA	-95 to -86	0.00047
Mouse *s2*	CAATGAAAAGATGA	-6 to +8	0.00244
Human	CAATGAAAAGATGA	+30 to +43	0.00273
Mouse *s3*	GCCAATTTCT	+110 to +119	0.00414
Human	GCCAATTTCC	+145 to +154	0.00198
Mouse *s4*	GTCATTTAGC	+262 to +271	0.00244
Human	GTCATTTAGC	+304 to +313	0.00244

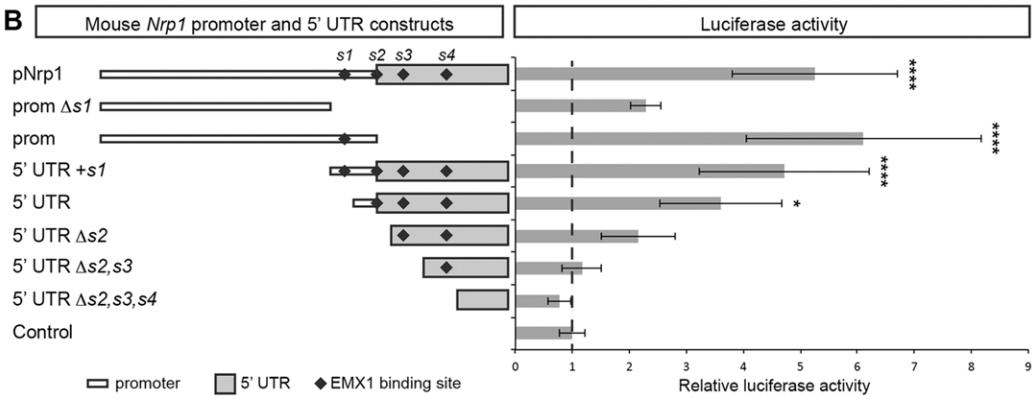

Fig. 7. EMX1 activates the transcription of *Nrp1 in vitro*. (A) Putative EMX1 binding sites conserved between the mouse and human *Nrp1* promoter and 5′ untranslated regions (5′ UTR). The monomeric and dimeric position weight matrices are ten and 14 base pairs, respectively. The positions of the EMX1 binding sites are shown in relation to the *Nrp1* transcriptional start site (+1). (B) Relative luciferase activity of mouse *Nrp1* promoter and 5′ UTR firefly luciferase constructs with EMX1 over-expression, normalized to the empty minimal promoter plasmid (Control). Results are mean±s.e.m. determined from a minimum of three independent experiments. **P*<0.05 and *****P*<0.0001 for one-way ANOVA with Dunnett's multiple comparisons test.

potentially be demonstrated to influence callosal dysgenesis in humans and mice.

NRP1/SEMA3C signaling is required for the midline crossing of callosal axons

Axon targeting and de-fasciculation defects that are due to a loss of NRP1/SEMA signaling are well documented for neocortical callosal axons *in vivo* (Gu et al., 2003; Hatanaka et al., 2009; Zhao et al., 2011; Zylbersztejn et al., 2012; Zhou et al., 2013). Together with recent studies (Niquille et al., 2009; Piper et al., 2009), our findings demonstrate that NRP1/SEMA signaling regulates similar events during the development of cingulate callosal axons. Interestingly, defects in callosal axon pathfinding and fasciculation have been hypothesized to also affect callosal targeting within the contralateral cortex (Zhou et al., 2013; Fenlon and Richards, 2015). Thus, whether *Emx1* knockout mice display defects in the final homotopic and heterotopic topography of callosal circuitry is of particular interest for further study.

EMX1 mediates cingulate callosal axon guidance by regulating *Nrp1* expression

The subtle phenotypes reported in *Emx1* knockout mice as well as conflicting reports regarding whether EMX1 regulates callosal development have masked the importance of EMX1 in the developing mouse brain (Qiu et al., 1996; Yoshida et al., 1997; Guo et al., 2000). Specifically, how EMX1 functions independently of EMX2, particularly within postmitotic cortical neurons, which only express EMX1 and not EMX2 (Gulisano et al., 1996), is poorly understood. The present study demonstrates a novel role for EMX1 in regulating cingulate callosal guidance by the upregulation of *Nrp1* expression. Even so, whether EMX1 binds to the *Nrp1* promoter *in vivo* to regulate *Nrp1* expression directly remains to be determined, as no anti-EMX1 antibodies have been reported for successful chromatin immunoprecipitation (including the antibodies we tested; see supplementary materials and methods). Our luciferase assays, however, suggest that EMX1 regulates *Nrp1* expression via transcriptional activation of the *Nrp1* promoter.

As EMX1 and NRP1 are expressed within both neocortical and cingulate callosal axons (Gulisano et al., 1996; Zhao et al., 2011; Zhou et al., 2013), the question that arises is why only a subpopulation of cingulate axons is misrouted in $Emx1^{-/-}$/C57Bl/6 mice. Further studies could investigate possible scenarios to explain this. Given that axonal growth cones integrate multiple cues to instruct pathfinding (Huber et al., 2003; O'Donnell et al., 2009), EMX1/*Nrp1* signaling might simply increase the probability of cingulate axons crossing the midline, rather than being an absolute requirement for these axons to reach the adjacent hemisphere. Thus, defective EMX1/*Nrp1* signaling in *Emx1* knockout mice would increase the probability of misguidance, with the most severely affected axons failing to project across the midline.

Alternatively, or in concert with the previous scenario, callosal pathfinding in unaffected axons might be regulated through guidance mechanisms that function irrespective of NRP1 signaling. For instance, the *Nrp1* homolog *Nrp2* is expressed in the anterior cingulate cortex of E15 $Emx1^{+/+}$/C57Bl/6 and $Emx1^{-/-}$/C57Bl/6 mice (see Fig. S2), and NRP2 is similarly responsive to SEMA3C during cortical development (Giger et al., 2000). Whether NRP2 functions as a compensatory factor in $Emx1^{-/-}$/C57Bl/6 mice is of interest for future study. In addition, we recently demonstrated that cingulate callosal axons also express the axon guidance receptor

Development (2015) 142, 3746-3757 doi:10.1242/dev.119909

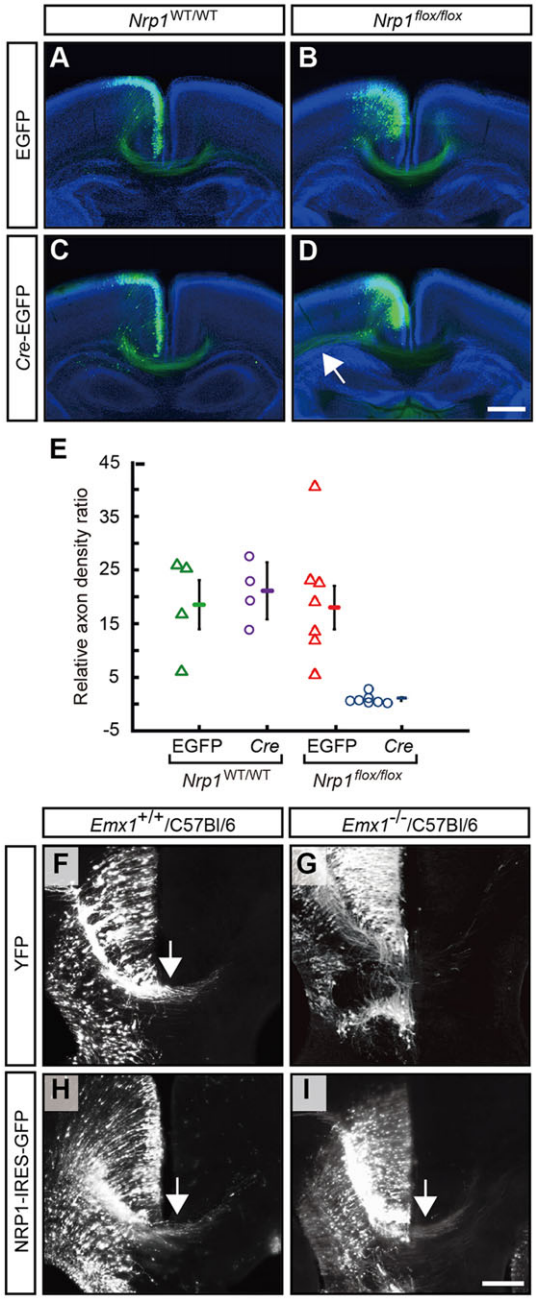

Fig. 8. Specific knockout of *Nrp1* in the cingulate cortex reduces the density of callosal axons crossing the midline, and re-expression of *Nrp1* in the cingulate cortex of *Emx1* knockout mice can increase callosal midline crossing. (A-D) A control EGFP construct or a *Cre*-EGFP construct was electroporated at E14.5 into the cingulate cortex of either $Nrp1^{flox/flox}$ mice (n=7 per condition) or their wild-type littermates (n=4 per condition). All animals were analyzed at P5. Arrow in D indicates cingulate axons projecting laterally in the $Nrp1^{flox/flox}$ mice electroporated with *Cre*-EGFP. (E) The axon density ratio (midline fluorescence normalized to ipsilateral fluorescence; results are mean±s.e.m.) demonstrates a significant reduction in axons crossing the midline with electroporation of *Cre*-EGFP in $Nrp1^{flox/flox}$ mice compared with all other conditions (P<0.05; one-way ANOVA with Tukey's multiple comparison post-test). (F-I) $Emx1^{+/+}$/C57Bl/6 and $Emx1^{-/-}$/C57Bl/6 littermates were electroporated with either a YFP or *Nrp1*-IRES-GFP expression plasmid in the cingulate cortex at E14 and sacrificed at E17. Shown are high-magnification views of the rostral cortical midline in coronal sections stained for YFP or GFP with arrows denoting midline crossing. Over-expression of *Nrp1* in $Emx1^{+/+}$/C57Bl/6 brains did not disrupt callosal axon crossing (arrow in H; 37 sections analyzed from n=7 animals). In $Emx1^{-/-}$/C57Bl/6 brains, fewer sections had callosal axons crossing the midline when only YFP was electroporated, but this was rescued when *Nrp1* was electroporated (arrow in I; 82 sections analyzed from n=18 animals for each condition). Scale bars: in D, 500 µm for A-D; in I, 10 µm for F-I.

DCC, and that these axons are attracted towards its ligand, NTN1, at the midline (Fothergill et al., 2014). Similarly, other short- and long-range axon guidance molecules have been demonstrated to function in regulating neocortical callosal pathfinding (Shu and Richards, 2001; Shu et al., 2003; Andrews et al., 2006; Islam et al., 2009; Nishikimi et al., 2011). As callosal axons from the dorso-lateral cortex, where *Nrp1* expression is absent, are able to project their axons medially (Zhou et al., 2013), it appears likely that other axon guidance mechanisms can guide callosal pathfinding in the absence of *Nrp1* expression.

Finally, EMX1 might be redundant in upregulating *Nrp1* expression within the neocortex. Although EMX2 is unlikely to compensate for EMX1 in neocortical callosal neurons as it is not expressed in these cells (Gulisano et al., 1996), the nuclear receptor NR4A2 is reportedly expressed within the cortex during callosal development, and has been suggested to act as a transcriptional activator of *Nrp1* (Zetterstrom et al., 1996; Hermanson et al., 2006). Whether NR4A2 compensates for the loss of EMX1 expression in $Emx1^{-/-}$/C57Bl/6 mice is therefore a question for future study.

Conclusions

The present study shows that EMX1 functions in corpus callosum development by specifically upregulating *Nrp1* expression within the anterior cingulate cortex. Uncovering this mechanism has established several important regulatory features for further study. First, genetic modifiers that differ between background strains of mice can modulate EMX1 function. Second, EMX1 is required for cingulate axon pathfinding and fasciculation at the midline, with *Emx1* mutants demonstrating the formation of aberrant axonal bundles. Finally, we have identified an animal model with specific anterior cingulate cortex wiring deficits that can be used in future studies to better understand the function of this circuit in behaviors such as depression and aggression.

MATERIALS AND METHODS

Animals

Animals were maintained on a 12 h dark/light cycle with food and water provided *ad libitum*. All experiments were approved by the animal ethics committee of The University of Maryland School of Medicine, The University of Queensland or the Institute of Neuroscience, Shanghai Institutes of Biological Sciences, Chinese Academy of Sciences. The *Emx1* knockout mice used were either on a mixed 129/SvJ/C57Bl/6 background (pre-backcrossed animals) or on a C57Bl/6 background (post-backcrossed). Post-backcrossed animals (*Emx1*/C57Bl/6) were generated by mating *Emx1* knockout mice (B6;129X1-$Emx1^{tm1Jir}$/J strain; Qiu et al., 1996) with C57Bl/6 wild-type partners. This was repeated for over ten generations, with selection to retain the *Emx1* mutation while alternating the C57Bl/6 wild type as the male or female between each generation. Heterozygotes from post-backcrossed animals were mated and the morning of the vaginal plug was designated E0. The *Emx1*-iCre; ROSA26CAG-lox-STOP-lox-tdTomato reporter mouse line was generated by crossing the *Emx1*-iCre mouse line (Kessaris et al., 2006) to the ROSA26CAG-lox-STOP-lox-tdTomato reporter mouse line obtained from the Jackson Laboratory (B6;129S6-$Gt(ROSA)26Sor^{tm9(CAG-tdTomato)Hze}$/J; Madisen et al., 2010). $Nrp1^{flox/flox}$ mice (Gu et al., 2003) were a gift from Prof. Alex Kolodkin (Johns Hopkins University, MD, USA) and were maintained on a C57Bl/6 background. Genotyping of *Emx1* knockout mice and $Nrp1^{flox/flox}$ mice was performed using PCR primers as previously described (Qiu et al., 1996; Gu et al., 2003).

Development (2015) 142, 3746-3757 doi:10.1242/dev.119909

Perfusion and tissue collection

Adult mice were anesthetized with an intraperitoneal injection of sodium pentobarbitone (Lethabarb; Virbac; 185 mg/kg body weight) in PBS. Postnatal animals were anesthetized on ice. For embryo perfusion, the pregnant dam was anesthetized and embryos were sequentially removed from the uterus. Mice were transcardially perfused with 0.9% saline solution (0.9% w/v NaCl in Milli-Q water; Merck Millipore) (1 minute for embryos and postnatal animals; 5 minutes for adults) followed by 4% w/v paraformaldehyde (PFA; ProSciTech) in PBS (4 minutes for embryos and postnatal animals; 15 minutes for adults). All brains were post-fixed in 4% PFA and stored at 4°C until analysis.

Immunohistochemistry and gold chloride staining

Fixed adult *Emx1*/C57BL/6 brains were bisected along the midline and immersed in gold chloride solution as previously described (Guo et al., 2000; Wahlsten et al., 2003). For immunohistochemistry, fixed brains were set in 3% w/v Noble agar (Difco; Becton Dickinson) in PBS. Brains were sectioned coronally at 45 µm thickness or 200 µm thickness (data for Fig. 8A-E only) using a vibratome (Leica). Sections were then stained with the relevant antibodies as described in the supplementary materials and methods.

Diffusion-weighted magnetic resonance imaging and tractography

HARDI and tractography were performed as previously described (Moldrich et al., 2011). Briefly, *Emx1* adult brains were incubated in 0.2% v/v Magnevist (Bayer HealthCare) over 4 days following fixation. Diffusion-weighted (DW) images were acquired with the brains immersed in Fomblin Y-LVAC fluid (Solvay Solexis), using a 16.4 Tesla vertical bore, small animal MRI scanner (Bruker Biospin; ParaVision v5.0) and a 15 mm linear surface acoustic wave coil (M2M Imaging). Three-dimensional 30 direction DW spin-echo sequences (b=5000 s/mm^2, 2×b=0) were acquired using the following parameters: repetition time=400 ms; echo time=22.8 ms; imaging resolution=0.1 mm isotropic. Reconstruction and tractography of the aberrant axonal bundles and equivalent callosal regions in controls were performed using Diffusion Toolkit and TrackVis (Ruopeng Wang and Van J. Wedeen, TrackVis.org, Martinos Center for Biomedical Imaging, Massachusetts General Hospital), according to the HARDI and Q-ball models (Hess et al., 2006). For characterization of homotopic callosal connectivity between the anterior cingulate, primary motor and primary somatosensory cortices, reconstruction and tractography was performed using MRtrix according to the constrained spherical deconvolution (CSD) model (Tournier et al., 2012). Cortical ROIs were defined by registering individual brains to a C57Bl/6J mouse neocortex atlas (Ullmann et al., 2013) using the FMRIB Software Library (Jenkinson et al., 2012). Tractography limits were set at FA values greater than 0.1 (fiber orientation density>0.1-0.25 for CSD tractography) and turning angle ≤45°.

Iontophoretic injection of anterograde tracer

Iontophoretic injection of the anterograde tracer was performed as previously described (Reiner et al., 2000), with an extended protocol delineated in the supplementary materials and methods. Briefly, an iontophoretic injector (Stoelting; 5 µA current pulses for 10 min; 7 s on, 7 s off) was used to deliver 15% w/v biotinylated dextran amine (10,000 MW; Life Technologies) in PBS into the anterior cingulate cortex through a glass micropipette (stereotactic coordinates: anterior posterior 1.42, lateral 0.2 and ventral −1.75).

In situ hybridization

In situ hybridization for *Nrp1* was performed using an antisense riboprobe as previously described (Piper et al., 2009) with minor modifications. The fluorescein-labeled probe was detected with anti-Fluorescein-AP, Fab fragments (Roche) and amplified for visualization with the TSA Plus Fluorescein System (PerkinElmer). Sections were then stained for immunofluorescence as described to amplify the tdTomato fluorescence signal. *In situ* hybridization for *Nrp2* was performed using a digoxygenin-labeled antisense riboprobe generated using the primers 5′-GCCTCTCTG-TCAAAAATGGATATG-3′ and 5′-GCGTAGTCTGAGGTGAACTTG-3′, and visualized with BM Purple (Roche).

Real-time quantitative PCR

RNA was isolated from E16 cingulate cortex using TRIzol reagent (Invitrogen). Reverse transcription was performed using SuperScript III First-Strand Synthesis SuperMix (Invitrogen) with Oligo(dT) primers. Real-time qPCRs were performed using a Rotor-Gene 3000 (Corbett Life Science) and Platinum SYBR Green qPCR SuperMix-UDG (Invitrogen) with the following thermocycler conditions: 2 min at 50°C and 2 min at 95°C, followed by 50 cycles with 15 s denaturation at 95°C and 30 s annealing and extension at 60°C. Relative expression was determined using the ΔΔCt method with *Actb* as a housekeeping gene. The *Nrp1* primers were 5′-GGTTTTCCATCCGCTATGAA-3′ and 5′-GGATTCGAGTCTTGCT-CCAG-3′, and the *Actb* primers were 5′-CACGATGGAGGGGAATACAG-3′ and 5′-CAGCTTCTTTGCAGCTCCTT-3′.

DNA constructs

In vitro co-culture axon guidance assay

The *Sema3C* expression construct in the pBK-CMV backbone was kindly provided by Prof. Andreas Püschel (Institut für Molekulare Zellbiologie, Westfälische Wilhelms-Universität Münster, Münster, Germany).

In utero electroporation

Plasmids of *ubiquitin-EGFP* and *ubiquitin-Cre-2A-GFP* were kindly provided by Prof. Zi-Long Qiu (Institute of Neuroscience, Chinese Academy of Sciences, Shanghai, China). Full-length *Nrp1* in the pCAG-IRES-GFP backbone was kindly provided by Prof. Alex Kolodkin (Johns Hopkins University, MD, USA).

In vitro co-culture axon guidance assay

The *in vitro* axon guidance assay was performed and analyzed as previously described (Piper et al., 2009). At the completion of the culture period, explants were fixed in 4% paraformaldehyde in PBS and stained with anti-neuronal-specific beta III tubulin antibody (TuJ1 clone) (1:1000; R&D Systems Cat# MAB1195) and goat anti-rabbit Alexa Fluor 488 secondary antibody (1:500; Invitrogen Cat# A11008).

Dual luciferase reporter assays

Ninety-six-well plates were individually seeded with 4500 U251 MG cells per well and maintained in DMEM (Life Technologies) supplemented with 10% v/v fetal bovine serum (SAFC Biosciences). After 24 h, a human or mouse *Nrp1* promoter plasmid (or the empty firefly luciferase control plasmid) was co-transfected with either pCAG-*Emx1*-IRES-GFP or pCAG-IRES-GFP into these cells. The *Renilla* luciferase vector pRL-SV40 was co-transfected as an internal control in all experiments. Cells were lyzed after 40 h and luciferase activity was measured using the Dual-Luciferase Reporter Assay System (Promega) on a POLARstar OPTIMA plate reader (BMG Labtech). Cloning of luciferase DNA constructs are described in Table S1 and the supplementary materials and methods.

In utero electroporation

In utero electroporation was performed as previously described (Saito, 2006). Briefly, pregnant mice were anesthetized with 90 mg/kg (body weight) ketamine (Parnell Laboratories, Australia) and 10 mg/kg xylazine (Troy Laboratories, Australia). An abdominal incision was made to expose the uterus, and plasmid DNA diluted in 0.5 µl PBS was injected through the uterine wall into the medial region of the lateral ventricle of the brain with a glass pipette. Electrical pulses (five 35 V pulses of 50 ms applied at 1 second intervals) were then delivered to embryos by electrodes connected to a square-pulse generator [either a CUY21 (BEX) for experiments in Fig. 7 or a ECM 830 electroporator (BTX Harvard Apparatus) for experiments in Fig. 8]. Embryos were returned into the abdominal cavity and the abdominal cavity was sutured until embryo perfusion.

Imaging and quantification

Imaging immunohistochemical and immunofluorescence material

Immunohistochemical images were obtained with a Zeiss Z1 microscope (Carl Zeiss), using bright-field illumination at 2.5× magnification for adult sections and 5× magnification for embryonic sections. Immunofluorescence

Development (2015) 142, 3746-3757 doi:10.1242/dev.119909

images were similarly obtained using 5× or 20× magnification. Gold chloride staining was imaged using a Zeiss Axiocam HrC camera (Carl Zeiss) attached to a stereodissecting microscope (Leica).

Axon density ratio analysis

Sections were first imaged using a fluorescence microscope (Nikon E600FN) equipped with a Plan Apo 10× objective to obtain an image over a large area. Images were also acquired at a higher resolution using a confocal microscope (Nikon A1R equipped with a 40×, NA 1.30 lens) and were stitched over a large area for each brain section. The axon density ratio of callosal axon projections at the midline was quantitatively analyzed using ImageJ software as previously described (Zhou et al., 2013). The axon density ratio was obtained as the axon density at the midline normalized to that of the ipsilateral hemisphere.

Acknowledgements

This article is dedicated to the late Prof. Giorgio Corte (National Institute for Cancer Research and Department of Oncology, Biology and Genetics, University of Genova Medical School) who provided important reagents for this project. We are also grateful to Prof. Alex Kolodkin, Prof. Andreas Püschel, Prof. David Ginty and Prof. Zi-Long Qiu for providing important mouse lines and reagents; the Australian Genome Research Facility, Dr J Bertran-Gonzalez, Dr Oressia Zalucki, Chantelle Reid, Ilse Buttiens, John Baisden, Kim Valentino and Sarah Croft for technical assistance; Sarah Preston and Lynette Knowles for early work on the project; and Laura Morcom and Rowan Tweedale for reading the manuscript and providing critical comments.

Competing interests

The authors declare no competing or financial interests.

Author contributions

J.W.C.L., A.-L.S.D., J.B., R.X.M., M.P., I.G., M.-M.P., J.L.R.R., and L.J.R. designed the experiments. J.W.C.L., A.-L.S.D., J.B., T.J.E., L.R.F., Y.L., J.Z., R.X.M. and T.L.B. performed experiments and analyzed the data. N.R.W. performed the statistical analysis of the rescue experiment. N.K. supplied the *Emx1*-iCre mouse line. J.W.C.L., A.-L.S.D. and L.J.R. conceived the project and wrote the manuscript. J.W.C.L., A.-L.S.D., T.J.E., J.Z. and R.X.M. prepared figures. All authors edited the manuscript.

Funding

This work was supported by a National Health and Medical Research Council of Australia (NHMRC) project grant [APP1043045 to L.J.R.]; a Chinese 973 Program grant [2011CBA00400 to M.-M.P.]; the National Institute of Neurological Disorders and Stroke at the National Institutes of Health [RO1NS34661 to J.L.R.R.]; an NHMRC Principal Research Fellowship (L.J.R.); an Australian Research Council Future Fellowship [FT120100170 to M.P.]; an NHMRC CJ Martin fellowship (R.X.M.); an International Postgraduate Research Scholarship and UQ Centennial Scholarship (J.W.C.L.); the Australian Postgraduate Award (A.-L.S.D. and L.R.F.); and the Queensland Brain Institute Top-Up Scholarship (J.W.C.L., A.-L.S.D. and L.R.F.). Deposited in PMC for release after 12 months.

Supplementary information

Supplementary information available online at
http://dev.biologists.org/lookup/suppl/doi:10.1242/dev.119909/-/DC1

References

Agroskin, D., Klackl, J. and Jonas, E. (2014). The self-liking brain: a VBM study on the structural substrate of self-esteem. *PLoS ONE* **9**, e86430.

Andrews, W., Liapi, A., Plachez, C., Camurri, L., Zhang, J., Mori, S., Murakami, F., Parnavelas, J. G., Sundaresan, V. and Richards, L. J. (2006). Robo1 regulates the development of major axon tracts and interneuron migration in the forebrain. *Development* **133**, 2243-2252.

Beck, J. A., Lloyd, S., Hafezparast, M., Lennon-Pierce, M., Eppig, J. T., Festing, M. F. W. and Fisher, E. M. C. (2000). Genealogies of mouse inbred strains. *Nat. Genet.* **24**, 23-25.

Bishop, K. M., Goudreau, G. and O'Leary, D. D. M. (2000). Regulation of area identity in the mammalian neocortex by Emx2 and Pax6. *Science* **288**, 344-349.

Bishop, K. M., Rubenstein, J. L. R. and O'Leary, D. D. M. (2002). Distinct actions of Emx1, Emx2, and Pax6 in regulating the specification of areas in the developing neocortex. *J. Neurosci.* **22**, 7627-7638.

Bishop, K. M., Garel, S., Nakagawa, Y., Rubenstein, J. L. R. and O'Leary, D. D. M. (2003). Emx1 and Emx2 cooperate to regulate cortical size, lamination, neuronal differentiation, development of cortical efferents, and thalamocortical pathfinding. *J. Comp. Neurol.* **457**, 345-360.

Choe, Y., Siegenthaler, J. A. and Pleasure, S. J. (2012). A cascade of morphogenic signaling initiated by the meninges controls corpus callosum formation. *Neuron* **73**, 698-712.

Dastot-Le Moal, F., Wilson, M., Mowat, D., Collot, N., Niel, F. and Goossens, M. (2007). ZFHX1B mutations in patients with Mowat-Wilson syndrome. *Hum. Mutat.* **28**, 313-321.

Edwards, T. J., Sherr, E. H., Barkovich, A. J. and Richards, L. J. (2014). Clinical, genetic and imaging findings identify new causes for corpus callosum development syndromes. *Brain* **137**, 1579-1613.

Fenlon, L. R. and Richards, L. J. (2015). Contralateral targeting of the corpus callosum in normal and pathological brain function. *Trends Neurosci.* **38**, 264-272.

Fothergill, T., Donahoo, A.-L. S., Douglass, A., Zalucki, O., Yuan, J., Shu, T., Goodhill, G. J. and Richards, L. J. (2014). Netrin-DCC signaling regulates corpus callosum formation through attraction of pioneering axons and by modulating Slit2-mediated repulsion. *Cereb. Cortex* **24**, 1138-1151.

Gasquoine, P. G. (2013). Localization of function in anterior cingulate cortex: from psychosurgery to functional neuroimaging. *Neurosci. Biobehav. Rev.* **37**, 340-348.

Giger, R. J., Cloutier, J.-F., Sahay, A., Prinjha, R. K., Levengood, D. V., Moore, S. E., Pickering, S., Simmons, D., Rastan, S., Walsh, F. S. et al. (2000). Neuropilin-2 is required in vivo for selective axon guidance responses to secreted semaphorins. *Neuron* **25**, 29-41.

Grant, C. E., Bailey, T. L. and Noble, W. S. (2011). FIMO: scanning for occurrences of a given motif. *Bioinformatics* **27**, 1017-1018.

Gu, C., Rodriguez, E. R., Reimert, D. V., Shu, T., Fritzsch, B., Richards, L. J., Kolodkin, A. L. and Ginty, D. D. (2003). Neuropilin-1 conveys semaphorin and VEGF signaling during neural and cardiovascular development. *Dev. Cell* **5**, 45-57.

Gulisano, M., Broccoli, V., Pardini, C. and Boncinelli, E. (1996). Emx1 and Emx2 show different patterns of expression during proliferation and differentiation of the developing cerebral cortex in the mouse. *Eur. J. Neurosci.* **8**, 1037-1050.

Guo, H., Christoff, J. M., Campos, V. E. and Li, Y. (2000). Normal corpus callosum in Emx1 mutant mice with C57BL/6 background. *Biochem. Biophys. Res. Commun.* **276**, 649-653.

Hatanaka, Y., Matsumoto, T., Yanagawa, Y., Fujisawa, H., Murakami, F. and Masu, M. (2009). Distinct roles of neuropilin 1 signaling for radial and tangential extension of callosal axons. *J. Comp. Neurol.* **514**, 215-225.

Hermanson, E., Borgius, L., Bergsland, M., Joodmardi, E. and Perlmann, T. (2006). Neuropilin1 is a direct downstream target of Nurr1 in the developing brain stem. *J. Neurochem.* **97**, 1403-1411.

Hess, C. P., Mukherjee, P., Han, E. T., Xu, D. and Vigneron, D. B. (2006). Q-ball reconstruction of multimodal fiber orientations using the spherical harmonic basis. *Magn. Reson. Med.* **56**, 104-117.

Huber, A. B., Kolodkin, A. L., Ginty, D. D. and Cloutier, J.-F. (2003). Signaling at the growth cone: ligand-receptor complexes and the control of axon growth and guidance. *Annu. Rev. Neurosci.* **26**, 509-563.

Islam, S. M., Shinmyo, Y., Okafuji, T., Su, Y., Naser, I. B., Ahmed, G., Zhang, S., Chen, S., Ohta, K., Kiyonari, H. et al. (2009). Draxin, a repulsive guidance protein for spinal cord and forebrain commissures. *Science* **323**, 388-393.

Jenkinson, M., Beckmann, C. F., Behrens, T. E. J., Woolrich, M. W. and Smith, S. M. (2012). FSL. *NeuroImage* **62**, 782-790.

Jolma, A., Yan, J., Whitington, T., Toivonen, J., Nitta, K. R., Rastas, P., Morgunova, E., Enge, M., Taipale, M., Wei, G. et al. (2013). DNA-binding specificities of human transcription factors. *Cell* **152**, 327-339.

Kessaris, N., Fogarty, M., Iannarelli, P., Grist, M., Wegner, M. and Richardson, W. D. (2006). Competing waves of oligodendrocytes in the forebrain and postnatal elimination of an embryonic lineage. *Nat. Neurosci.* **9**, 173-179.

Kim, B. S., Lee, J., Bang, M., Seo, B. A., Khalid, A., Jung, M. W. and Jeon, D. (2014). Differential regulation of observational fear and neural oscillations by serotonin and dopamine in the mouse anterior cingulate cortex. *Psychopharmacology* **231**, 4371-4381.

Madisen, L., Zwingman, T. A., Sunkin, S. M., Oh, S. W., Zariwala, H. A., Gu, H., Ng, L. L., Palmiter, R. D., Hawrylycz, M. J., Jones, A. R. et al. (2010). A robust and high-throughput Cre reporting and characterization system for the whole mouse brain. *Nat. Neurosci.* **13**, 133-140.

Mallamaci, A., Muzio, L., Chan, C.-H., Parnavelas, J. and Boncinelli, E. (2000). Area identity shifts in the early cerebral cortex of Emx2-/- mutant mice. *Nat. Neurosci.* **3**, 679-686.

Meechan, D. W., Rutz, H. L. H., Fralish, M. S., Maynard, T. M., Rothblat, L. A. and LaMantia, A.-S. (2015). Cognitive ability is associated with altered medial frontal cortical circuits in the LgDel mouse model of 22q11.2DS. *Cereb. Cortex* **25**, 1143-1151.

Miller, A. R., Hawkins, N. A., McCollom, C. E. and Kearney, J. A. (2014). Mapping genetic modifiers of survival in a mouse model of Dravet syndrome. *Genes Brain Behav.* **13**, 163-172.

Moldrich, R. X., Pannek, K., Hoch, R., Rubenstein, J. L., Kurniawan, N. D. and Richards, L. J. (2010). Comparative mouse brain tractography of diffusion magnetic resonance imaging. *NeuroImage* **51**, 1027-1036.

Moldrich, R. X., Mezzera, C., Holmes, W. M., Goda, S., Brookfield, S. J., Rankin, A. J., Barr, E., Kurniawan, N., Dewar, D., Richards, L. J. et al. (2011). Fgfr3 regulates development of the caudal telencephalon. *Dev. Dyn.* **240**, 1586-1599.
Niquille, M., Garel, S., Mann, F., Hornung, J.-P., Otsmane, B., Chevalley, S., Parras, C., Guillemot, F., Gaspar, P., Yanagawa, Y. et al. (2009). Transient neuronal populations are required to guide callosal axons: a role for semaphorin 3C. *PLoS Biol.* **7**, e1000230.
Nishikimi, M., Oishi, K., Tabata, H., Torii, K. and Nakajima, K. (2011). Segregation and pathfinding of callosal axons through EphA3 signaling. *J. Neurosci.* **31**, 16251-16260.
O'Donnell, M., Chance, R. K. and Bashaw, G. J. (2009). Axon growth and guidance: receptor regulation and signal transduction. *Annu. Rev. Neurosci.* **32**, 383-412.
Ozaki, H. S. and Wahlsten, D. (1998). Timing and origin of the first cortical axons to project through the corpus callosum and the subsequent emergence of callosal projection cells in mouse. *J. Comp. Neurol.* **400**, 197-206.
Paul, L. K., Brown, W. S., Adolphs, R., Tyszka, J. M., Richards, L. J., Mukherjee, P. and Sherr, E. H. (2007). Agenesis of the corpus callosum: genetic, developmental and functional aspects of connectivity. *Nat. Rev. Neurosci.* **8**, 287-299.
Pellegrini, M., Mansouri, A., Simeone, A., Boncinelli, E. and Gruss, P. (1996). Dentate gyrus formation requires Emx2. *Development* **122**, 3893-3898.
Piper, M., Plachez, C., Zalucki, O., Fothergill, T., Goudreau, G., Erzurumlu, R., Gu, C. and Richards, L. J. (2009). Neuropilin 1-Sema signaling regulates crossing of cingulate pioneering axons during development of the corpus callosum. *Cereb. Cortex* **19** Suppl. 1, i11-i21.
Probst, M. (1901). Ueber den Bau des vollständig balkenlosen Gross-hirnes sowie über Mikrogyrie und Heterotopie der grauen Substanz. *Arch. Psychiatr. Nervenkr.* **34**, 709-786.
Qiu, M., Anderson, S., Chen, S., Meneses, J. J., Hevner, R., Kuwana, E., Pedersen, R. A. and Rubenstein, J. L. R. (1996). Mutation of the Emx-1 homeobox gene disrupts the corpus callosum. *Dev. Biol.* **178**, 174-178.
Rash, B. G. and Richards, L. J. (2001). A role for cingulate pioneering axons in the development of the corpus callosum. *J. Comp. Neurol.* **434**, 147-157.
Reiner, A., Veenman, C. L., Medina, L., Jiao, Y., Del Mar, N. and Honig, M. G. (2000). Pathway tracing using biotinylated dextran amines. *J. Neurosci. Methods* **103**, 23-37.
Ren, T., Anderson, A., Shen, W.-B., Huang, H., Plachez, C., Zhang, J., Mori, S., Kinsman, S. L. and Richards, L. J. (2006). Imaging, anatomical, and molecular analysis of callosal formation in the developing human fetal brain. *Anat. Rec. A Discov. Mol. Cell. Evol. Biol.* **288A**, 191-204.
Ren, T., Zhang, J., Plachez, C., Mori, S. and Richards, L. J. (2007). Diffusion tensor magnetic resonance imaging and tract-tracing analysis of Probst bundle structure in Netrin1- and DCC-deficient mice. *J. Neurosci.* **27**, 10345-10349.
Richards, L. J., Plachez, C. and Ren, T. (2004). Mechanisms regulating the development of the corpus callosum and its agenesis in mouse and human. *Clin. Genet.* **66**, 276-289.
Saito, T. (2006). In vivo electroporation in the embryonic mouse central nervous system. *Nat. Protoc.* **1**, 1552-1558.
Schaefer, G. B., Bodensteiner, J. B., Buehler, B. A., Lin, A. and Cole, T. R. P. (1997). The neuroimaging findings in Sotos syndrome. *Am. J. Med. Genet.* **68**, 462-465.
Sellers, R. S. (2012). The gene or not the gene–that is the question: understanding the genetically engineered mouse phenotype. *Vet. Pathol.* **49**, 5-15.
Shinozaki, K., Miyagi, T., Yoshida, M., Miyata, T., Ogawa, M., Aizawa, S. and Suda, Y. (2002). Absence of Cajal-Retzius cells and subplate neurons associated with defects of tangential cell migration from ganglionic eminence in Emx1/2 double mutant cerebral cortex. *Development* **129**, 3479-3492.
Shinozaki, K., Yoshida, M., Nakamura, M., Aizawa, S. and Suda, Y. (2004). Emx1 and Emx2 cooperate in initial phase of archipallium development. *Mech. Dev.* **121**, 475-489.
Shu, T. and Richards, L. J. (2001). Cortical axon guidance by the glial wedge during the development of the corpus callosum. *J. Neurosci.* **21**, 2749-2758.
Shu, T., Sundaresan, V., McCarthy, M. M. and Richards, L. J. (2003). Slit2 guides both precrossing and postcrossing callosal axons at the midline in vivo. *J. Neurosci.* **23**, 8176-8184.
Tamamaki, N., Fujimori, K., Nojyo, Y., Kaneko, T. and Takauji, R. (2003). Evidence that Sema3A and Sema3F regulate the migration of GABAergic neurons in the developing neocortex. *J. Comp. Neurol.* **455**, 238-248.
Toth, M., Tulogdi, A., Biro, L., Soros, P., Mikics, E. and Haller, J. (2012). The neural background of hyper-emotional aggression induced by post-weaning social isolation. *Behav. Brain Res.* **233**, 120-129.
Tournier, J.-D., Calamante, F. and Connelly, A. (2012). MRtrix: diffusion tractography in crossing fiber regions. *Int. J. Imag. Syst. Technol.* **22**, 53-66.
Tuch, D. S. (2004). Q-ball imaging. *Magn. Reson. Med.* **52**, 1358-1372.
Ullmann, J. F. P., Watson, C., Janke, A. L., Kurniawan, N. D. and Reutens, D. C. (2013). A segmentation protocol and MRI atlas of the C57BL/6J mouse neocortex. *NeuroImage* **78**, 196-203.
van den Buuse, M., Martin, S., Holgate, J., Matthaei, K. and Hendry, I. (2007). Mice deficient in the alpha subunit of G(z) show changes in pre-pulse inhibition, anxiety and responses to 5-HT(1A) receptor stimulation, which are strongly dependent on the genetic background. *Psychopharmacology* **195**, 273-283.
Vogt, B. A. (2005). Pain and emotion interactions in subregions of the cingulate gyrus. *Nat. Rev. Neurosci.* **6**, 533-544.
Vogt, B. A. and Paxinos, G. (2014). Cytoarchitecture of mouse and rat cingulate cortex with human homologies. *Brain Struct. Funct.* **219**, 185-192.
Wahlsten, D., Colbourne, F. and Pleus, R. (2003). A robust, efficient and flexible method for staining myelinated axons in blocks of brain tissue. *J. Neurosci. Methods* **123**, 207-214.
Weber, R., Ritterfeld, U. and Mathiak, K. (2006). Does playing violent video games induce aggression? Empirical evidence of a functional magnetic resonance imaging study. *Media Psychol.* **8**, 39-60.
Yamashita, H., Zeredo, J. L., Kaida, K., Kimoto, M., Asahina, I. and Toda, K. (2013). Stress-induced modulation of nociceptive responses in the rat anterior cingulate cortex. *J. Integr. Neurosci.* **12**, 235-246.
Yoshida, M., Suda, Y., Matsuo, I., Miyamoto, N., Takeda, N., Kuratani, S. and Aizawa, S. (1997). Emx1 and Emx2 functions in development of dorsal telencephalon. *Development* **124**, 101-111.
Zetterstrom, R. H., Williams, R., Perlmann, T. and Olson, L. (1996). Cellular expression of the immediate early transcription factors Nurr1 and NGFI-B suggests a gene regulatory role in several brain regions including the nigrostriatal dopamine system. *Brain Res.* **41**, 111-120.
Zhao, H., Maruyama, T., Hattori, Y., Sugo, N., Takamatsu, H., Kumanogoh, A., Shirasaki, R. and Yamamoto, N. (2011). A molecular mechanism that regulates medially oriented axonal growth of upper layer neurons in the developing neocortex. *J. Comp. Neurol.* **519**, 834-848.
Zhou, J., Wen, Y., She, L., Sui, Y.-N., Liu, L., Richards, L. J. and Poo, M.-M. (2013). Axon position within the corpus callosum determines contralateral cortical projection. *Proc. Natl. Acad. Sci. USA* **110**, E2714-E2723.
Zylbersztejn, K., Petkovic, M., Burgo, A., Deck, M., Garel, S., Marcos, S., Bloch-Gallego, E., Nothias, F., Serini, G., Bagnard, D. et al. (2012). The vesicular SNARE Synaptobrevin is required for Semaphorin 3A axonal repulsion. *J. Cell Biol.* **196**, 37-46.

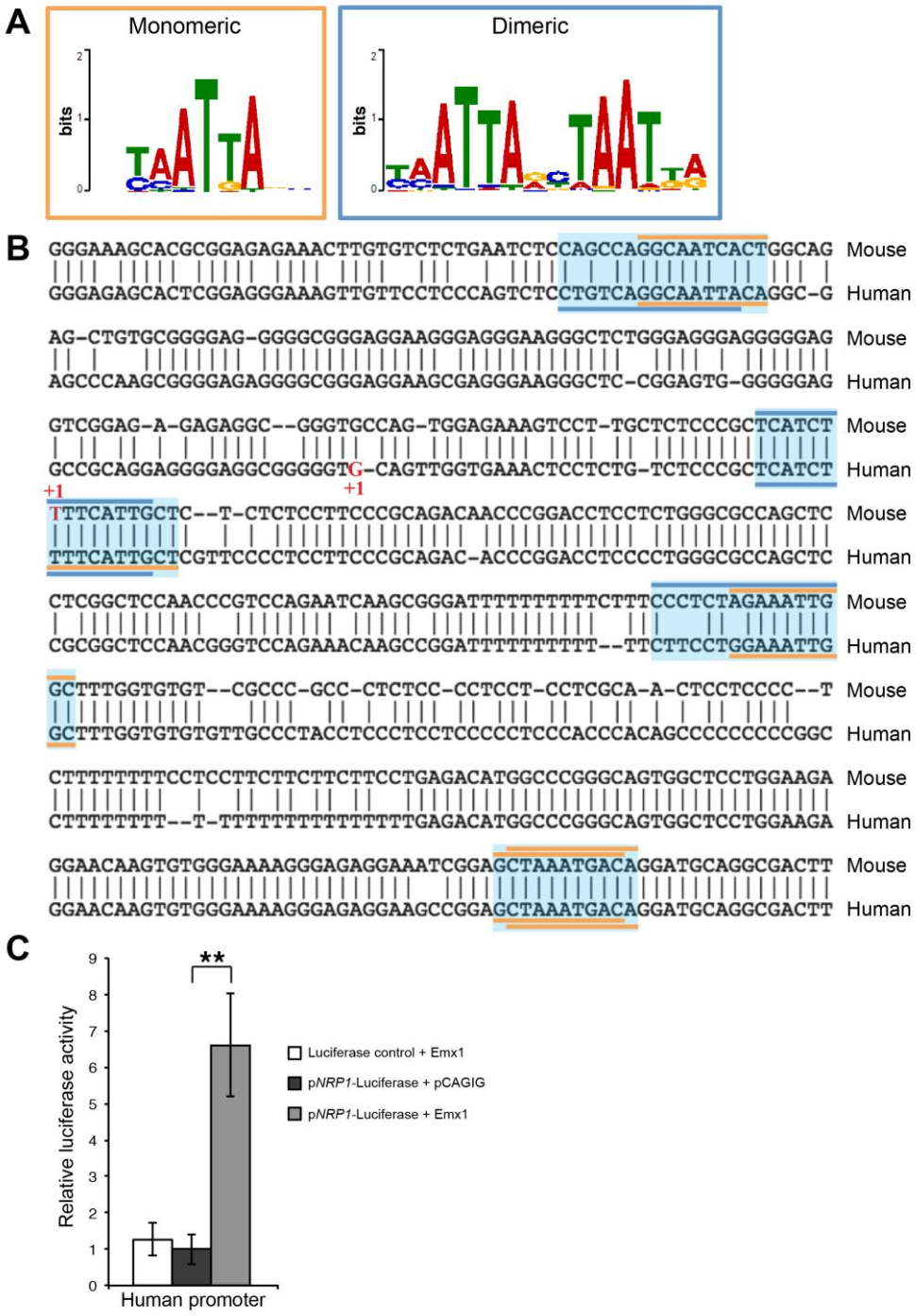

Figure S1: EMX1 over-expression up-regulates human *NRP1* promoter activity. Monomeric and dimeric consensus EMX1 binding sites represented as position weight matrices (EMX1_DBD and EMX1_DBD_2 respectively from Jolma et al., 2013) were used to identify putative EMX1 binding sites within the mouse and human *Nrp1* promoter and untranslated regions (A). In a 643 base pair region of the mouse

Nrp1 locus (chr8:130,882,800-130,883,258 obtained from NCBI37/mm9) that is conserved in humans (chr10:33,623,535-33,623,944 obtained from GRCh37/hg19) with 83% identity, four highly conserved sequences (shaded blue) with EMX1 binding sites were identified (B). Either monomeric (orange lines) or dimeric (blue lines) consensus EMX1 binding sites were detected at identical positions in the mouse and human promoters ($p<0.01$). Nucleotides in red, denoted +1, represent the respective transcriptional start sites. Dual-luciferase reporter assays demonstrate significant activation of the human *NRP1* promoter with EMX1 over-expression, normalized to over-expression of the empty pCAG-IRES-GFP control (C). ** $p<10^{-6}$ for two-sided Student's *t*-test. Results are mean±s.d. from $n=3$ independent experiments.

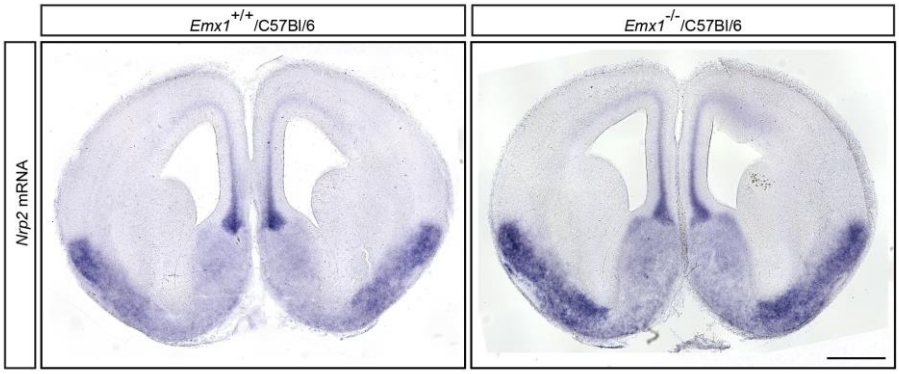

Figure S2: *Nrp2* mRNA is expressed in the anterior cingulate cortex of *Emx1*$^{+/+}$/C57Bl/6 and *Emx1*$^{-/-}$/C57Bl/6 mice. *Nrp2 in situ* hybridization in coronal brain sections from E15 *Emx1*$^{+/+}$/C57Bl/6 and *Emx1*$^{-/-}$/C57Bl/6 mice (minimum *n*=3 per genotype). Scale bar = 500 μm.

Table S1: Cloning primers for generating mouse *Nrp1* promoter constructs.

Name (see Fig. 7 for schematic)	Forward primer	Reverse primer
pNrp1	5'-TATAACTAGTCTGGCACTAGGAGACCCTTG-3'	5'-TATACTCGAGCCCCTCTCCATCCTCCTTC-3'
prom Δ*s1*	5'-TATAACTAGTCTGGCACTAGGAGACCCTTG-3'	5'-TATACTCGAGTTTCTCTCCGCGTGCTTTC-3'
prom	5'-TATAACTAGTCTGGCACTAGGAGACCCTTG-3'	5'-TATACTCGAGAAGATGAGCGGGAGAGCAAG-3'
5' UTR +*s1*	5'-TATACTCGAGTTTCTCTCCGCGTGCTTTC-3'	5'-TATACTCGAGCCCCTCTCCATCCTCCTTC-3'
5' UTR	5'-TATAACTAGTAAGGGAGGGAAGGGCTCTG-3'	5'-TATACTCGAGCCCCTCTCCATCCTCCTTC-3'
5' UTR Δ*s2*	5'-TATAACTAGTCAACCCGTCCAGAATCAAGC-3'	5'-TATACTCGAGCCCCTCTCCATCCTCCTTC-3'
5' UTR Δ*s2,s3*	5'-TATAACTAGTCTTCCTGAGACATGGCCC-3'	5'-TATACTCGAGCCCCTCTCCATCCTCCTTC-3'
5' UTR Δ*s2,s3,s4*	5'-TATAACTAGTCTCGCGAATTCAGGCATTG-3'	5'-TATACTCGAGCCCCTCTCCATCCTCCTTC-3'

Supplementary Materials and Methods

Immunohistochemistry

All incubations were performed at room temperature on a rotator. Sections were washed in PBS for 30 minutes, after which they were incubated in blocking solution (2% v/v normal goat serum (Vector Laboratories) or normal donkey serum (Jackson Laboratories); 0.2% v/v Triton X-100, in PBS) for 2 hours. They were then incubated overnight with the primary antibody diluted in blocking solution. Primary antibodies and the concentrations used were: mouse anti-Neurofilament (145 kDa; 1:50000 for floating immunohistochemistry and 1:500 for immunofluorescence; EMD Millipore Cat# MAB1621), mouse anti-GAP43 (1:100000; EMD Millipore Cat# AB5220), rabbit anti-NRP1 (1:50000; a gift from Prof. David Ginty, Johns Hopkins University, MD, USA), rabbit anti-EMX1 (provided by Prof. Giorgio Corte, University of Genova Medical School, Genova, Italy), rabbit anti-DsRed (1:500; Clontech Cat# 632496; for amplification of tdTomato fluorescence signal following *Nrp1 in situ* hybridization) and rabbit anti-GFP (1:500; Invitrogen Cat# A6455).

Sections were washed in PBS for 1 hour before incubating with secondary antibody for 1 hour. Secondary antibodies used for fluorescence analysis were either donkey anti-rabbit Alexa Fluor 546 (1:500; Invitrogen Cat# A-10040) or donkey anti-mouse Alexa Fluor 488 (1:500; Invitrogen Cat# A-21202). Biotinylated dextran amine was fluorescently labeled with Streptavidin, Alexa Fluor 555 conjugated (1:500; Invitrogen Cat# S-32355). Sections stained for fluorescence were coverslipped using ProLong Gold antifade reagent (Invitrogen). Secondary antibodies for chromogenic immunohistochemistry analysis were biotinylated goat anti-rabbit (1:500; Vector Laboratories Cat# BA-1000), biotinylated donkey anti-mouse (1:500; Jackson Laboratories Cat# 715-065-150) or biotinylated donkey anti-goat (1:500;

Jackson Laboratories Cat# 705-065-003), diluted in PBS containing 0.2% v/v Triton X-100. Sections were washed for 1 hour in PBS and then incubated for 1 hour in an avidin-biotin complex solution (0.2% v/v Triton X-100, avidin (A) [1:500] and biotin (B) [1:500] (VECTASTAIN Elite ABC kit, Vector Laboratories) in PBS). After a 30-minute wash in PBS, sections were transferred to a nickel-3'3'-diaminobenzidine tetrahydrochloride (DAB) color reaction solution (95 mM $NiSO_4$, 175 mM CH3COONa.3H_2O, 0.56 mM DAB (Sigma-Aldrich), 0.0025% v/v hydrogen peroxide solution). Sections were observed until staining was visible. The color reaction was stopped by returning the sections to PBS. Sections were mounted in serial order onto gelatinized glass slides and dried at room temperature. They were then dehydrated through an ethanol series (70% v/v, 95% v/v, and 2x 100%) and clearing agents (3x Histo-clear; National Diagnostics) for at least 1 minute each. Coverslips were added using DPX neutral mounting medium (Ajax Finechem).

Extended protocol for iontophoretic injection of anterograde tracer

Adult mice were anesthetized with 3% isoflurane in oxygen (flowrate of 1 L/minute) and maintained under anesthesia with 1% isoflurane in oxygen (1 L/minute). The anesthetized mouse was placed in a stereotactic frame (David Kopf Instruments) and a small incision was made to expose the skull. A small hole was made through the skull using a 27.5 gauge needle, through which the biotinylated dextran amine was iontophoretically injected. A retention current was applied when inserting and removing the glass micropipette from the injection site, with the micropipette left in place for 2 minutes before and after the injection. All animals were perfused 4 days after tracer injection.

Cloning of DNA constructs for luciferase assays

Emx1 mouse cDNA (NCBI Reference Sequence: NM_010131.2) was obtained from OriGene Technologies and fused at its C-terminus to a HA-tag epitope. The HA-tagged *Emx1* construct was re-cloned into pCAG-IRES-GFP at the EcoRI and NotI restriction sites and verified by sequencing. The pSGG_prom firefly luciferase construct driven by ~1kb of the human *NRP1* promoter was obtained from SwitchGear Genomics. The empty pSGG_prom control vector was constructed by removing the *NRP1* promoter at the MluI and BglII restriction sites and ligating the digested ends using the Quick Blunting and Quick Ligation Kits (New England Biolabs). Primers used to clone the mouse *Nrp1* promoter and 5' UTR regions are listed in supplementary material Table S1. Forward primers were designed to contain a SpeI restriction site and the reverse primers contained an XhoI restriction site. The *Nrp1* promoter constructs was cloned to drive firefly luciferase expression from the pGL4.23 plasmid (Promega) using the NheI and XhoI restriction sites.

Validation of antibodies for chromatin immunoprecipitation

We tested the following three commercial antibodies as described below: Santa Cruz Biotechnology Cat# sc-28220; Abcam Cat# ab82901; Abcam Cat#32925. Firstly, antibodies were tested for immunohistochemistry and immunofluorescence on brain sections of *Emx1*/C57Bl/6 wildtype and knockout mice. Secondly, we over-expressed a HA-tagged EMX1 construct in HEK293T cells and performed chromatin immunoprecipitation (ChIP) with 5 µg of antibody and 200 µg Pierce Protein G Magnetic Beads (Thermo Scientific). Following ChIP, the antibodies and proteins bound to the magnetic beads were denatured for western blot, with blots stained using an anti-HA tag antibody (Cell Signaling Technology Cat# 2367). All three antibodies failed both tests in all instances.

Supplementary References

Jolma, A., Yan, J., Whitington, T., Toivonen, J., Nitta, K. R., Rastas, P., Morgunova, E., Enge, M., Taipale, M., Wei, G. et al. (2013). DNA-binding specificities of human transcription factors. *Cell* **152**, 327-339.